STATISTICS OF COHERENT STRUCTURES IN TURBULENT FLUID FLOW

by

STUART REID LOEWEN

B.Sc.,the University Of Manitoba,1980

A THESIS SUBMITTED IN PARTIAL FULFILMENT OF

THE REQUIREMENTS FOR THE DEGREE OF

MASTER OF SCIENCE

in

THE FACULTY OF GRADUATE STUDIES

Physics Department

We accept this thesis as conforming

to the required standard

THE UNIVERSITY OF BRITISH COLUMBIA

December 1983

In presenting this thesis in partial fulfilment of the requirements for an advanced degree at the University of British Columbia, I agree that the Library shall make it freely available for reference and study. I further agree that permission for extensive copying of this thesis for scholarly purposes may be granted by the head of my department or by his or her representatives. It is understood that copying or publication of this thesis for financial gain shall not be allowed without my written permission.

Department of Physics

The University of British Columbia
1956 Main Mall
Vancouver, Canada
V6T 1Y3

Date 30 December 1983

Abstract

This thesis compares power spectra produced from hot-film anemometery measurements in turbulent flow with those generated from the distribution of eddy sizes obtained from photographs of the same flow. The coherent structures were made visible by photographing the paths of aluminum tracers on the surface of a water filled towing tank. A parallel row of bars was used to generate the turbulent flow. Flow Reynold's numbers, based on bar spacing, of about 20,000 were studied.

A simple analysis of the flow patterns photographed proved adequate to predict power spectra consistent with those measured using a hot-film anemometer and spectrum analyzer. The frequency range and shape of the eddy power spectra were similar to the hot-film ones but were consistently lower in magnitude. The integral length scales obtained from the power spectra agree within 30% and it was found that the average eddy size predicted the length scale obtained from the eddy produced power spectra. Successive photographs of the flow as well as the change in the eddy size distributions with distance from the grid showed evidence of eddy evolution. The results of this thesis suggest that new knowledge and understanding of the interaction of coherent structures in a turbulent fluid flow can be obtained from such flow visualization experiments.

This study is part of a new model for turbulence in which the flow is described as a superposition of coherently

rotating eddies and laminar flow. In this model we attempt to derive macroscopic properties of a turbulent flow from the interactions of eddies with the fluid, fluid flow and each other. The eddy size distribution can also be predicted from an understanding of the eddy interactions.

The statistical description of turbulence and the often used k -power spectrum approach are reviewed and compared with our new model.

Table of Contents

Abstract ii
List of Figures v
List of Figures vi
Acknowledgement vii

Chapter I
INTRODUCTION 1

Chapter II
STATISTICAL DESCRIPTION OF TURBULENCE 9
2.1 Motivation And Introduction 9
2.2 Statistical Spectra 11
2.3 Correlations And Spectra 16
2.4 Velocity Fluctuations And The Power Spectrum 23

Chapter III
GRID TURBULENCE EXPERIMENTS 27
3.1 Introduction 27
3.2 The Tank 29
3.3 The Grid 32
3.4 Visualization Apparatus 32
3.5 The Search For Coherent Structures 34
3.6 Hot-film Apparatus 44
3.7 Hot-film Power Spectra 48

Chapter IV
EDDY-SIZE DISTRIBUTIONS AND HOT-FILM SPECTRA 56
4.1 Introduction 56
4.2 Eddy-Size Spectra 58
4.3 Generation Of E (w) From N(R) 67
4.4 Power Spectrum Obtained From U(t) 71
4.5 Results And Discussion 81

Chapter V
CONCLUSIONS 93

BIBLIOGRAPHY 96

APPENDIX A - HOT-FILM PROBE SENSITIVITY TO VELOCITY FLUCTUATIONS 97

APPENDIX B - RIGID BODY EDDY VELOCITY PROFILE 98

APPENDIX C - TURB.FTN FORTRAN CODE 99

APPENDIX D - AVERAGE EDDY CHORD AND PEDDY CALCULATION ...102

List of Figures

1. Correlation Velocities 17
2. Spatial Correlation Curve 18
3. Flow Field Past Probe 20
4. The Towing Tank 28
5. Optical Detector and Timer 31
6. Lights and Camera Action 33
7. Flow Visualization in Grid and Fluid Frames 36
8. Visualizations at Different Shutter Speeds 37
9. 20cm/sec Flow Photographs 40
10. 30cm/sec Flow Photographs 41
11. 40cm/sec Flow Photographs 42
12. 50cm/sec Flow Photographs 43
13. Hot-Film Power Spectrum Schematic 46
14. Hot-Film Linearization 51
15. Hot-Film Oscillograms 52
16. Probe Support Resonance 55
17. Typical Analyzer X-Y Plot 55
18. Power Spectra Comparison 57
19. Eddy Analysis 59
20. Eddy Angular Velocities 62
21. 30cm/sec Eddy-Size Spectra 63
22. 40cm/sec Eddy-Size Spectra 65
23. N(R) to E (w) Computation 68
24. u(t) Generated from the Eddy Distribution 70
25. Eddy Power Spectra 72

26. Eddy Power Spectra: Variation with Distance 73
27. Spectrum Analyzer Operation 76
28. Analyzer X-Y Plot 78
29. Hot-Film Power Spectra: Variation with Distance 79
30. Eddy Pairing 82
31. Comparison of Length Scales 89
32. Eddy Count with Distance 89
33. Variation in Occupied Area 90
34. Decay of $\overline{u^2}$ 90
35. Comparison of Power Spectra 91
36. Equivalent Area Representation 92

Acknowledgement

I would like to thank Paul Burrel who machined and designed things that worked and Al Cheuck for building the timer and getting supplies "now would be best". Helping hands and minds of summer assistants Norman Lo, who made the tank that "will not leak" (and eventually did not), Alex Filuik who got the visualization system underway and Peter Smereka of "Fine Idea" fame. The loan of the CTA unit from Dr.Quick of the UBC Civil Engineering Dept. is much appreciated. Although not directly referenced the teaching of Dr.I.Gartshore of the UBC Mechanical Engineering Dept. provided a solid appreciation for what is known about fluid flows. I would also like to thank the UBC Plasma Physics group for continuing to work one floor beneath the tank filled with three tons of water. Finally I would like to thank my supervisor Dr.B.Ahlborn for his enthusiastic help in both the research and writing aspects of this thesis.

I. INTRODUCTION

This thesis investigates the role of coherent structures in a turbulent fluid flow. It is supposed that a turbulent flow can be described as a superposition of coherently rotating fluid elements, 'eddies', plus laminar flow. These eddies are taken as the building blocks of the fluctuating flow field. Experiments performed to test the validity and viability of this model are presented.

The individual eddies interact with the fluid, the local flow field and with each other according to the fluid equations of motion. We characterize the turbulent fluid flow by the eddy-size spectrum which is the probability of seeing an eddy of a given size at a point in space. This probability is determined by the mechanics of the interaction processes. The model is thus deterministic on small time and space scales while being stochastic on larger time and space scales. This approach has the potential of describing small scale coherence as well as large scale unpredictability which are significant properties of turbulent flows. (e.g. the weather)

In order to develop an understanding of the eddy dynamics and statistics the relationship between our eddy-size spectrum and the well known power spectral density description of the fluctuating flow field was studied. The power spectral density is a measure of the energy content in the fluctuating flow as a function of temporal frequency. It can be related to the wave number spectrum through the

convection velocity. The wavenumber spectrum gives the energy content in the fluctuating flow field as a function of scale size. How these spectra are used in the statistical description of turbulent velocity fluctuations is described in the second chapter.

The relationship between the eddy-size distribution and the power spectral density was studied for a number of reasons. The power spectral density is conveniently obtained using a constant temperature anemometer and spectrum analyzer and has long been used to study the length scales present in turbulent flows. Its relationship to the coherent structures in the turbulent flow is neither intuitive nor clearly defined. Our statistical analysis of the turbulent elements on the other hand is simple in concept, but still somewhat subjective in the analysis. This thesis will show how the power spectral density can be obtained from both the eddy-size distribution and from hot-film anemometery measurements. In comparing the procedures, assumptions and the results we hope to convince the reader of the usefulness of our approach. A computer code was written and used to generate power spectra from eddy spectra. This procedure is described in detail.

An experimental study of grid generated turbulence in water was performed. This mechanism for generating turbulent flow was selected so as to obtain a large volume of turbulent flow with spatially homogeneous properties. It was also anticipated that the grid geometery would create a

flow that would evolve independently of boundary conditions. A towing tank was used as it allowed for easy access to both the fluid and the object reference frames for photographic and hot-film anemometry studies.

The flow was visualized by photographing the motion of tracer particles on the surface of the water. With the camera mounted in the fluid reference frame we were pleasantly surprised by the profusion of coherent structures of a broad size range. The photographs were analyzed to obtain the eddy-size distributions as well as the angular velocities of the eddies. Although of large uncertainty the angular velocity data was consistent with our treating the eddies as performing solid body rotation. The same flow situations were studied by measuring one dimensional power spectra using hot wire anemometery and a spectrum analyzer. Power spectral density curves were predicted from the eddy spectra and compared with those more directly obtained using a hot-film anemometer and spectrum analyzer. Inspiration for studying coherent structures using the towing tank came from photographic results obtained by F.Ahlborn.[1]

While the main topic of this thesis is the comparison of different statistical descriptions of turbulent flow it is an integral part of a broader concept developed by

---

[1] F.Ahlborn:"Turbulenz und Mechanismus desWiderstandes an Kugeln und Zylindern", Zeitschrift fur Technische Physik 12, 482-491 (1931).

B.Ahlborn and myself.[1] We attempt to explain many facets of turbulence based on the interactions of idealized coherent elements in fluid flow. We call these idealized elements "vortons". Central to the vorton model is the prediction of the eddy-size spectrum from the vorton dynamics. It was therefore important for the success of the vorton model that the coherent structures could be observed and counted by size. It was also important to show that the information contained in the eddy distribution was consistent with a power spectral density description of the turbulent fluctuations. A general introduction to the vorton model is presented as it provided the motivation for performing the present statistical study.

> "Big whorls have little whorls,
> Which feed on their velocity;
> Little whorls have smaller whorls,
> And so on unto viscosity."

This information laden poem was written by L.F.Richardson, (1922). It introduces several concepts which our vorton model addresses. Firstly, turbulent fluid flow is characterized by the presence of a broad range in size scales of the motion. Our model incorporates this as

---

[1] UBC PLASMA PHYSICS lab report #89

the presence of different sizes of eddies in the flow. Secondly, turbulent flows are generally thought to feed energy into large eddies through shear stresses in the mean flow field. The strain produced by the larger eddies in turn feeds energy into the smaller scales, typically by "vortex stretching" or "tearing". The whole process is commonly called the "energy cascade". Our model starts with the assumption that a turbulent flow field can be described as being a composite of eddies and laminar flow. We then define rates for an eddy's interaction with the fluid, the laminar flow field, and other eddies. These interactions are found to dominate the eddy dynamics in the small scale or dissipative regime, the large scale regime and the medium eddy size or collisional regime, respectively. We then use these rates to solve for the distribution of eddy size scales. This distribution we call the eddy-size spectrum. Richardson's poem brings out that the energy transfer ultimately ends in producing heat through viscous dissipation. In our model this is quantified according to the energy loss rate through viscous dissipation as a function of eddy size. We also show how this spectrum can be used to predict macroscopic properties of a particular turbulent flow. These properties include drag forces, wake sizes, diffusion processes, the onset of turbulence and mean velocity profiles.

The name vorton is chosen to indicate that we are dealing with a vortical structure which contains energy and

can interact with its flow environment. Vortons are treated as being excited states of a fluid flow. The word eddy is sometimes used interchangably with 'vorton. The eddy-size spectrum is interpreted as the probability of observing an eddy as a function of eddy size. This spectrum is central to our description of turbulence. It can be a function of space as well as time. Supporting the eddy-size spectrum are other properties of the eddies, such as their internal velocity distributions, convection velocities both in the flow dirction and normal to it, and if we are considering three dimensional flow, their orientations in space.

It is supposed that just as the eddies can be isolated and characterized, so can physical processes which produce, evolve, and finally destroy the eddies. In the first applications of the model the vortons have a circular cylindrical symmetry and are treated as being part of a two dimensional flow. We divide the possible interactions a vorton can take part in into three main types. A vorton may interact with the fluid surrounding it, with the fluid flow in which it is embedded or with other vortons. The rate at which a given vorton state changes, to other states, is described by a rate equation with coefficients quantifying the various interaction processes. We use A coefficients to describe the rate at which the number of eddies of a given size will spontaneously decay to eddies of a different size through viscous interaction with the fluid surrounding it. B coefficients are used to describe the rate at which a

population of eddies of a given size will either increase or decrease due to interaction with the local fluid flow field. This rate is goverened by tearing and vortex stretching dynamics. C coefficients are used to describe the population changes due to eddies interacting with other eddies, i.e. collisional processes. These rate coefficients are supposed derivable from the local physical processes which are goverened by the fluid equations of motion. The C coefficients incorporate collisional statistics as well. Although derived from local deterministic physics these coefficients are treated as probabilities which determine the populations of energy states. If the rates are known one can write a complete set of rate equations, one for each vorton state in the system, to predict the eddy-(or vorton) size spectrum. We thus see our model as a quantification of the eddy cascade process. It is important to note that in a turbulent fluid flow their will in general be a continuous distribution of eddy enrgies and sizes. Although in its infant stages the vorton model only deals with discrete sizes and energies a continuous version could be based on similar principals.the same We use the vorton description to model the flow in the hope that our idealization can describe the phenomenon and has some relation to the physics of a real turbulent flow.

It is generally accepted that different physical processes dominate the flow dynamics in different scale regimes. Standard texts on turbulence describe the large

scale motions as being associated with energy transfer from the mean flow with these size scales making up the "production" regime. The mid-size scales which comprise the inertial,inviscid, or Kolmogorov regime are collision dominated and the small scale motions which comprise the dissipative regime are most efficient at losing energy to heat. In the light of our model we would say that the B coefficients dominate the eddy dynamics in the production regime, the C coefficients dominate in the inertial regime and the A coefficients dominate in the dissipative regime.

In the interest of keeping the model simple and managable in its infant stage its applications have been confined to two dimensional flow phenomena. One can, in principal, apply these ideas to three dimensional flow situations.

The rate equation approach has been borrowed from the description of atomic ionization phenomena. This approach is a significant departure from main stream turbulence theory. It was conceived and developed by B.Ahlborn and myself in part based on flow photographs and some ideas of F.Ahlborn.

II. STATISTICAL DESCRIPTION OF TURBULENCE

2.1 Motivation And Introduction

We assert that the eddy spectrum description contains all the information needed to recreate a physically meaningful fluctuating flow field. The eddy spectrum based description should thus be sufficient to predict all the statistical fluctuation spectra. A description of these spectra and how they apply to the study of turbulent fluid flow is the subject of this chapter. These spectra include the power spectral density, three dimensional wave number spectrum and spectra based on higher order moments of the time or space varying velocity field. The often studied correlation curves are Fourier transforms of the above mentioned spectra and so would be equally well predicted by the eddy spectrum description. The inter-eddy correlations may or may not be significant, depending on the flow situation studied and the eddy size scale being considered. If we believe that the primary coherent structures represent all of the correlations present in the flow, meaningful flow fields should be reproducible from the eddy spectrum description. This description should also provide predictions of the macroscopic flow properties such as drag, wake sizes, diffusion processes, turbulence onset and mean velocity profiles.

A good test of the validity and viability of a statistically based coherent structures model of turbulent

flow would be to see if it predicts the correct power spectral density curves for a given flow. The power spectral density is a measure of the energy content per unit mass associated with the temporal frequency. This spectrum can be obtained by Fourier analyzing a time dependent velocity signal. In an experimental study of turbulence the time varying quantity could be the streamwise component of the fluctuating velocity field measured at a fixed position in relation to the object which is creating the turbulence. This description of the fluctuating velocity field contains information on the eddy cascade dynamics and the eddy statistics only implicitly. In the words of J.L.Lumley, "An eddy, however, is associated with many Fourier coefficients and the phase relations among them. Fourier transforms are used because they are convenient (spectra can be measured easily); more sophisticated transforms are needed if one wants to decompose a velocity field into eddies instead of waves."[1] Our approach is to predict turbulent effects from the distribution of the eddies.

This chapter describes the statistical fluctuation spectra and how the power spectral density can be obtained from a fluctuating velocity.

---

[1] Lumley,J.L.,1970.
Stochastic tools in turbulence.Academic Press,New York.

2.2 Statistical Spectra

In the statistical study of turbulent fluctuations one tries to predict and determine the velocity fluctuation spectra or, equivalently, the correlations. There are many texts which describe this approach in detail. Here I will present enough information to show how the power spectral density fits in a more complete statistical description of turbulent fluctuations and how it can be obtained and used to describe turbulent flows.

The starting point of the statistical description of turbulence is to consider the time dependent velocity $U(\vec{x},t)$ and pressure $P(\vec{x},t)$ fields as the sum of steady and unsteady components.

$$U_i(\vec{x},t)=\overline{U_i}(\vec{x})+u_i(\vec{x},t) \quad i=1,2,3 \qquad (2\text{-}1a)$$

$$P(\vec{x},t)=\overline{P}(\vec{x})+p(\vec{x},t) \qquad (2\text{-}1b)$$

Here $\overline{U_i}(\vec{x})$ and $\overline{P_i}(\vec{x},t)$ are the time averaged quantities and $u_i(\vec{x},t)$ and $p_i(\vec{x},t)$ are the fluctuating components. The overbar symbol is used to denote a time average. For some time dependent quantity $a(t)$, $\overline{a}(t)$ is found as,

$$\overline{a}(t)=\lim_{T\to\infty}\frac{1}{T}\int_{t'=t}^{t+T}dt'a(t') \qquad (2\text{-}2)$$

It is meaningful to speak of time dependent time averages if

$$(d/dt)[\overline{a}(t)] << \sqrt{\overline{(d/dt)[a(t)]^2}} \qquad (2\text{-}3)$$

which states that the averages must change much more slowly than the average change. In the rest of this thesis it will be assumed that the flow fields being dealt with are

statistically steady.[1]

The representation (2-1) for the fluid flow and pressure fields is next substituted into the appropriate fluid equations of motion to obtain equations for the mean kinetic energy, turbulent[2] kinetic energy, and the Reynolds normal and shear stress equations. For incompressible, isothermal, viscous fluid flow the appropriate equations of motion are the well known Navier-Stokes equations. In component form with the summation convention being used these equations are

$$\frac{\partial U_i}{\partial t} + U_j \frac{\partial U_i}{\partial x_j} = (-1/\rho)\frac{\partial P}{\partial x_i} + \nu \frac{\partial^2 U_i}{\partial x_k \partial x_k} \qquad (2\text{-}4)$$

with the continuity condition

$$\frac{\partial U_j}{\partial x_j} = 0 \qquad (2\text{-}5)$$

The time averaged Navier-Stokes equations are found by substituting eqns.(2-1) into eqn.(2-4) and time averaging the result is

$$\frac{D\overline{U}_i}{Dt} = -\frac{1}{\rho}\frac{\partial \overline{P}}{\partial x_i} + \frac{\partial}{\partial x_k}\left(\nu \frac{\partial \overline{U}_i}{\partial x_k} - \overline{u_i u_k}\right) \qquad (2\text{-}6)$$

Where $\frac{D}{Dt}U_i \left(= \frac{\partial U_i}{\partial t} + U_j \frac{\partial U_i}{\partial x_j}\right)$ is the time rate of change of U_i following the fluid motion. Multiplying this equation by $\overline{U}_i$, using the continuity condition, eqn.(2-5), to

---

[1] Statistically steady is used here to mean time averaged quantities do not change in time.

[2] A less misleading name for this equation would be the fluctuation kinetic energy

consolidate velocity components inside the derivatives[1], and recognizing that $U_i \frac{DU_i}{Dt} = \frac{D(\frac{1}{2}U_i U_i)}{Dt}$ we arrive at the mean kinetic energy equation for turbulent flow,

$$\frac{D}{Dt}\tfrac{1}{2}(\overline{U_i}\,\overline{U_i}) = -\frac{\partial}{\partial x_i}(\overline{U}\overline{P}/\rho) - \overline{U}\frac{\partial}{\partial x_k}(\overline{u_i u_k}) + \nu\overline{U_i}\frac{\partial^2 \overline{U_i}}{\partial x_k^2} \qquad (2\text{-}7)$$

(A) (B) (C) (D)

Term (D) may be rewritten as

$$\nu\overline{U_i}\frac{\partial^2 \overline{U_i}}{\partial x_k^2} = \nu\frac{\partial}{\partial x_k^2}(\overline{U_i}^2/2) - \nu\left(\frac{\partial \overline{U_i}}{\partial x_k}\right)^2 \qquad (2\text{-}8)$$

(D) (E) (F)

These equations state:

The time rate of change (A) of mean kinetic energy of a unit mass of fluid is equal to (B) the pressure work done on the unit mass, plus (C) the transport of mean energy by orthogonal velocity fluctuation correlations, plus (E) the change due to viscous gradient diffusion, plus (F) the mean viscous dissipation.

The turbulent kinetic energy equation is found by multiplying the original Navier-Stokes equations (2-4) by U_i, substituting the expressions (2-1) for U_i and P_i and then time averaging the result. The mean kinetic energy equation (2-7) is then subtracted from this and after some consolidation the turbulent kinetic energy equation results

$$\frac{\partial \frac{1}{2}\overline{u_k^2}}{\partial t} = -\frac{\partial}{\partial x_i}\overline{u_i\left(p/\rho + \tfrac{1}{2}u_k^2\right)} - \overline{u_i u_j}\frac{\partial \overline{U_j}}{\partial x_i} + \nu\frac{\partial}{\partial x_i}\overline{u_j\left(\frac{\partial u_i}{\partial x_j} + \frac{\partial u_j}{\partial x_i}\right)} \qquad (2\text{-}9)$$

(A) (B) (C) (D)

$$-\nu\overline{\left(\frac{\partial u_i}{\partial x_j} + \frac{\partial u_j}{\partial x_i}\right)\frac{\partial u_j}{\partial x}} \quad \text{(E)}$$

---

[1] i.e. $U_j \frac{\partial}{\partial x_j}U_i \Rightarrow \frac{\partial}{\partial x_j}(U_i U_j)/2$ as $\frac{\partial u_i}{\partial x_i} = 0$ from continuity

The following quote, taken from Hinze,[1] describes the physical meaning of the terms appearing in this equation.

> "The change (A) in kinetic energy of turbulence per unit of mass of the fluid is equal to (B) the convective diffusion by turbulence of the total turbulence energy,plus (C) the energy transferred from the mean motion through the turbulence shear stresses,or the production of turbulence energy, plus (D) the work done per unit of mass and of time by the viscous shear stresses of the turbulent motion, plus (E) the dissipation per unit of mass by the turbulent motion."

In a manner similar to that used above, equations for the Reynold's shear ($\overline{u_i u_j}$, $i \neq j$) and normal ($\overline{u_\alpha u_\alpha}$, no summation) stresses can be derived. The velocity fluctuation correlations in these equations are mostly of second order. Equations involving higher order correlations of the fluctuating velocity components are seldom used due to their mathematical complexity, inconvenience in measurement and lack of intuitive physical meaning.

One advantage of treating the velocity and pressure fields as the sum of a mean and fluctuating component is that the quantities appearing in the resulting equations are

---

[1] TURBULENCE,J.O.Hinze; McGRAW-HILL, 1959, pp 65

experimentally measureable using hot-wire or laser doppler anemometery techniques.[1] Another advantage is that the individual terms have some physical meaning. A major drawback of this approach is that in some cases this physical interpretation can be misleading. The average fluid velocity at a given point in space may be partially comprised of coherently adding fluctuations. For example, a turbulent boundary layer may contain coherent structures with a preferred rotation sense. The fluctuation in velocity measured when a series of coherent structures were convected past an anemometer would contribute constructively to the measurement of the mean velocity. Thus the interpretation of the mean and fluctuating velocities must be treated with caution. In discussing the mean kinetic energy equation (2-7) the significance of orthogonal fluctuating velocity correlations to the transport of mean kinetic energy was mentioned. A non-zero correlation implies a coherence between the two fluctuating velocities which would point to the presence of coherent structures in the turbulent flow. These structures, now thought to be important to the dynamics of most turbulent flows are not directly addressed in the above approach. It should be noted that these structures are the starting point of our

---

[1] In the stress equations the pressure fluctuation-velocity fluctuation correlations are not generally measureable and must be inferred from the stress equations and measurements of the other terms.

model.

The gain in writing the velocity field as the sum of mean and fluctuating components is that the correlations and mean values are quantities which have a useful, although potentially misleading, physical significance and they are readily measured with hot-wire or laser doppler anemometry techniques. It is important to note that in writing the velocity and pressure fields as the sum of the steady and fluctuating components we no longer have a closed system of equations. Since the number of unknowns has doubled an originally closed description has now been become incomplete. Closure hypotheses are needed to solve the new equations of motion.

2.3 Correlations And Spectra

The turbulent energy equation contains only mean products of fluctuating quantities at one point in space. To study the length scales of the turbulent fluctuations we need to consider fluctuating quantities which are measured at different points in space. Usually no more than two-point correlations are considered. The most general, statistically steady, two-point spatial correlation between fluctuating velocity components may be written

$$C_{ij}(\vec{x},\vec{r})=\overline{u_i(\vec{x},t)u_j(\vec{x}+\vec{r},t)} \qquad i,j=1,2,3 \qquad (2\text{-}10)$$

where $\vec{x}$ is the position where the correlation is defined, u_i is the fluctuating component of the velocity in the i direction, and $\vec{x}+\vec{r}$ is the position where the jth velocity

component is measured, see figure 1.

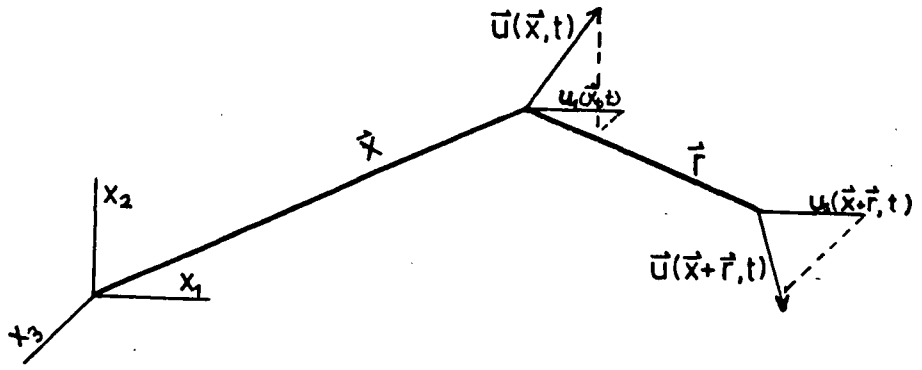

Figure 1 - Correlation Velocities

The non-dimensionalized correlation is called the correlation coefficient and is given as

$$R_{ij}(\vec{x},\vec{r}) = \frac{u_i(\vec{x},t)\,u_j(\vec{x}+\vec{r},t)}{\sqrt{u_i^2(\vec{x},t)}\sqrt{u_j^2(\vec{x}+\vec{r},t)}} \qquad (2\text{-}11)$$

$\tilde{R}$ forms a second rank tensor whose individual components are such that

$$-1 < R_{ij}(\vec{x},\vec{r}) < 1 \quad i,j=1,2,3 \qquad (2\text{-}12)$$

This agrees with the interpretation that R_{ij} is a measure of the degree of correlation between the two velocity components. A typical spatial correlation curve for identical velocity components appears in figure 2.

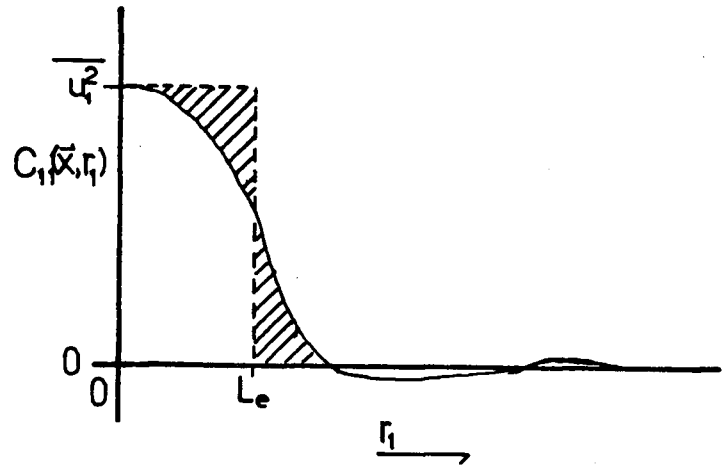

Figure 2 - Spatial Correlation Curve

At $\vec{r}=0$ we see from eqn.(2-11) above that $R_{ii}=1$ $i=1,2,3$. It is a property of turbulent flows that fluctuating velocity components are uncorrelated for sufficiently large distances and so we have

$$R_{ij}(\vec{x},\vec{r}) \Rightarrow 0 \quad \text{for large } |\vec{r}| \qquad (2\text{-}13)$$

If the mean fluid velocity measured at $\vec{x}$ is in, say, the x_1 direction then $R_{11}(r_1)$ is called the 'longitudinal spatial correlation coefficient' and $R_{22}(r_1)$ and $R_{33}(r_1)$ are 'lateral spatial correlation coefficients'. A simple measure of the length scale of the energy containing fluctuations is given by

$$Le=\int_{r_1=0}^{\infty} R_{11}(r_1')\,dr_1' \qquad (2\text{-}14)$$

called the integral length scale, see figure 2.

In some flow situations a useful measure of the length

scales in the fluctuations can be found from the temporal correlations. The auto-correlation curve is the average product of the same quantity measured as a function of separation time T,

$$C_{aa}(T)=\overline{u_a(\vec{x},t)u_a(\vec{x},t+T)} \qquad a=1,2 \text{ or } 3 \qquad (2\text{-}15)$$

This curve is much more easily obtained from experiment than the space correlations discussed above. Only one velocity measuring probe, a correlator and a signal delay unit are needed. The auto-correlation curve is obtained by sweeping the delay time T rather than physically moving a velocity probe. The time scale of the energy containing fluctuations, the integral time scale Te, is defined as

$$Te=1/\overline{u^2}\int_{T'=0}^{\infty}C(T')dT' \qquad (2\text{-}16)$$

The auto-correlation is useful in the study of turbulent fluctuations when it can be related to the spatial correlations. This relatationship and the conditions of its applicability are discussed below.

Consider a flow field moving past a velocity probe, figure 3.

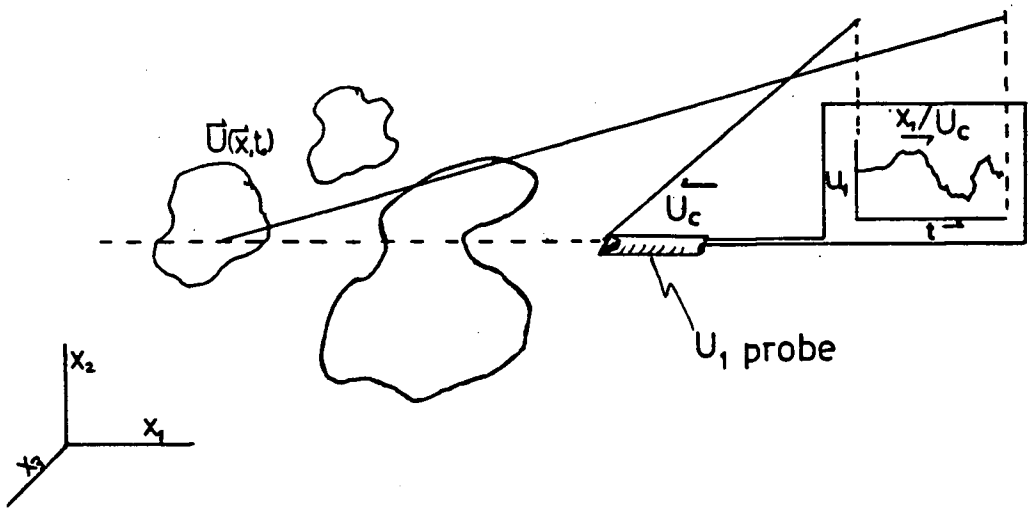

Figure 3 - Flow Field Past Probe

Assume the convection speed is the same for all fluid elements and the coherent structures do not change appreciably in the time it takes them to flow past the probe. The probe measures the velocity as a function of time. The space correlation is obtained from the time correlation of the temporally varying signal by simply multiplying the time axis of the auto-correlation by the probe speed, Uc.

$$C_{ab}(T)=C_{ab}(X/Uc) \quad a,b=1,2,3 \qquad (2-17)$$

The integral time scale can thus be related to the integral length scale by the relation,

$$Te=Le/Uc \qquad (2-18)$$

This co-ordinate transformation and the conditions when it can be applied is called, "Taylor's hypothesis" after G.I.Taylor. The important point to note is that Taylor's hypothesis can only be applied when the flow field does not

change appreciably during the time it takes the velocity measuring probe to sample a distance greater than the length scale of interest. In addition the fluid elements must have a constant convection velocity, Uc.

Just as a fluctuating flow field can be described by the spatial correlations we can describe it by the Fourier transforms of the correlations without loss of information. The Fourier transform of the spatial correlation tensor is called the three dimensional wave vector spectrum,

$$\Phi_{ij}(\vec{k},\vec{x})=[1/(2\pi)^3]\int_v u_i(\vec{x},t)u_j(\vec{x}+\vec{r},t)\exp(i\vec{k}\cdot\vec{r})d\vec{r} \qquad (2\text{-}19)$$

with $|\vec{k}|=2\pi/\lambda$ being the wave number. Experimentally it is impractical to measure all velocity components needed to define this spectrum.

One spectrum which is often used in both theory and experiment is the k_1-wave number spectrum which is found from $\Phi_{ij}(\vec{k},\vec{x})$ as

$$\Phi_{11}(\vec{k},\vec{x})=\int_{k_2=k_3=-\infty}^{\infty}\Phi_{11}(\vec{k},\vec{x})dk_2\,dk_3 \qquad (2\text{-}20)$$

It is twice the total of all kinetic energies per unit mass of the velocity fluctuations in the x_1 direction, having wave number between $k_1-dk_1/2$ and $k_1+dk_1/2$.

In the experimental study of grid turbulence described in the following chapters the most convenient quantity to measure was the power spectral density of the u fluctuating component, $E_{11}(w,\vec{x})$. $E_{11}(w,\vec{x})$ is twice the u_1 component of the kinetic energy per unit mass associated with temporal

frequency w.[1] It can be obtained by Fourier analyzing the fluctuating velocity component $u_1(\vec{x},t)$ measured with a directionally sensitive probe at a fixed position $\vec{x}$. $C_{11}(w)$ and $E_{11}(w)$ as defined above form a cosine transform pair,

$$E_{11}(w)=4\int_0^\infty C_{11}(T)\cos(2\pi wT)dT \qquad (2\text{-}21a)$$

$$C_{11}(T)=\int_0^\infty E_{11}(w)\cos(2\pi wT)dw \qquad (2\text{-}21b)$$

The limits of integration are from 0 to ∞ as $E_{11}(w)=E_{11}(-w)$ and $C_{11}(T)=C_{11}(-T)$. From eqn.(2-21b) we see that

$$C_{11}(0)=\int_0^\infty E_{11}(w)dw \qquad (2\text{-}22)$$

And using the expression of eqn.(2-15) for the autocorrelation,

$$\overline{u_1^2}=\int_0^\infty E_{11}(w)dw \qquad (2\text{-}23)$$

This equation identifies the total fluctuating kinetic energy $\overline{u_1^2}$ with the area under the power spectral density curve.

Applying Taylor's hypothesis to the power spectral density measurement we arrive at the relation

$$\Phi_{11}(\vec{k},\vec{x})=Uc/(2\pi)E_{11}(w,\vec{x}) \qquad (2\text{-}24)$$

The power spectral density is related to the k_1-wave number spectrum $\Phi_{11}(\vec{k},\vec{x})$ through the longitudinal convection velocity U_c at which the probe samples the flow field in the same way as the spatial and temporal correlations are. This

---

[1] It should be noted that the symbol w is to denote the frequency and not the angular frequency as is commonly done.

includes the same restrictive assumptions, namely that the convection velocity U is constant and that the flow does not change appreciably while the probe samples a distance greater than the length scales of interest. Using eqn.(2-16) in eqn.(2-21a) for w=0 we see,

$$E_{11}(0)=4\overline{u_1^2}\,Te \qquad (2\text{-}25)$$

And applying Taylor's hypothesis in the form of eqn.(2-18) we see that the integral length scale can be obtained from the power spectral density $E_{11}(w)$ as

$$Le=UcE_{11}(0)/(4\overline{u_1^2}) \qquad (2\text{-}26)$$

2.4 Velocity Fluctuations And The Power Spectrum

The power spectrum E(w) which is defined in terms of the transform of the correlation can be obtained directly from a Fourier transform of the fluctuating velocity. [1] To see this we first write the time dependent longitudinal fluctuating velocity $u_1(t)$ in its Fourier representation,

$$u_1(t)=2\int_{-\infty}^{\infty} dn[a(n)\cos(2\pi nt)+b(n)\sin(2\pi nt)] \qquad (2\text{-}27)$$

a(n) and b(n) are the Fourier coefficients for the basis functions of frequency n,

$$a(n)=1/\pi\int_{-\infty}^{\infty} dt\; u_1(t)\cos(2\pi nt) \qquad (2\text{-}28a)$$

$$b(n)=1/\pi\int_{-\infty}^{\infty} dt\; u_1(t)\sin(2\pi nt) \qquad (2\text{-}28b)$$

---

[1] from TURBULENCE,J.O.Hinze;McGRAW-HILL, 1959, pp 54-58

The auto-correlation coefficient for the longitudinal velocity fluctuations is,

$$C_{11}(T)=\overline{u_1(t)u_1(t+T)} \qquad (2\text{-}29)$$

Inserting the Fourier representation for $u_1(t)$, eqns.(2-28), into this expression and performing some of the integrations we have

$$\overline{u_1(t)u_1(t+T)}=\lim_{\tau\to\infty}\int_0^{\tau} dm[a^2(m)+b^2(m)]/\tau \cos(2\pi mt) \qquad (2\text{-}30)$$

and

$$\overline{u^2}=\lim_{\tau\to\infty}\int_0^{\tau} dm[a^2(m)+b^2(m)]/\tau \qquad (2\text{-}31)$$

where τ is the sampling time. If we now identify $E_{11}(n)$ with the cosine transformed quantity in eqn.(2-30) for t=0,

$$E_{11}(n)=\pi^2[a^2(m)+b^2(m)]/\tau \qquad (2\text{-}32)$$

we may write

$$R_{11}(T)=1/\overline{u^2}\int_0^{\infty} dnE_{11}(n)\cos(2\pi nt) \qquad (2\text{-}33)$$

and comparing this with eqn. (2-21b) we see that the two expressions, (2-32) and (2-21a) for $E_{11}(w)$ are equivalent . It was more convenient to obtain $E_{11}(w)$ from a Fourier analysis of the velocity field directly than by first obtaining the autocorrelation. Equation (2-32) tells us how to do this in the continuous case. In this thesis we use the fluctuation spectra defined as in eqn.(2-32) to compare our eddy-size spectra description of turbulent fluctuations with the fluctuations measured using a hot-film anemometer.

The standard methods used to predict the evolution of a turbulent flow field are either based on the turbulent kinetic energy equation (2-9) , or similarly the Reynolds stress equations, or k_{11} -wave number spectrum,equation (2-

20). Both approaches need closure hypotheses to be solved as in writing the velocity and pressure fields as the sum of an average and a fluctuating component the number of unknowns has doubled without increase in the number of equations. To close the kinetic energy equation (2-9) one needs assumptions about how the stress and velocity derivatives are related. In the case of the $k_{\parallel}$-wave number spectrum one must know the energy transfer function which describes how processes at one frequency will affect the amplitude at another frequency. Again model assumptions are invoked which are dictated more by mathematical expedience than by insight into the physical processes dictating the flow evolution. In both cases it is the details of the collective, or coherent, effects which is added to complete the description.

Our approach is to model the interaction of the coherent structures directly. We seek to derive the rate coefficients that describe the eddy evolution from the fluid equations of motion. These rates are then used to describe properties of the flow such as the eddy size distribution. Our model is much like the $k_{\parallel}$- wave number approach except that it more naturally accounts for the coherent structure dominated energy transfer mechanisms so that any assumptions can be based on the physics of the interactions rather than the mathematics of the wave number spectra.

The aim of this thesis is to show that coherent structures exist in a turbulent flow and that their size

distribution can be measured and can be used to predict the power spectra of velocity fluctuations in a turbulent flow. This study is based on experimental observations of grid turbulence.

III. GRID TURBULENCE EXPERIMENTS

3.1 Introduction

For the study of the statistics of coherent structures a simple and reliable method to generate and observe turbulent flow was needed. The towing tank and grid apparatus shown in figure 4 were chosen for several reasons. First, we wanted to see if coherent structures could be observed and measured with a photographic technique. Second, we wanted to see if these structures could be meaningfully described in a simple eddy-size spectrum. Third, we wanted to compare this description with the power spectral density measured using a velocity probe. The working fluid was chosen to be water for versatility in the flow visualization technique.

A towing tank was chosen rather than a water tunnel for the following reasons. With a towing tank both the fluid and object reference frames are easily accessible for measurements. Diagnostic equiptment such as cameras can be mounted in the lab frame. Hot-film probes and cameras can also be mounted on the cart which moves the grid through the water. A towing tank has arbitrarily quiescent 'upstream' conditions. It also does not have problems of boundary layer buildup along the walls. A disadvantage of any tank is its finite length which limits the observation time $T = L/U$; here L is the useable cart travel distance and U is the cart speed. The towing tank built for this study had a

length of 16'.

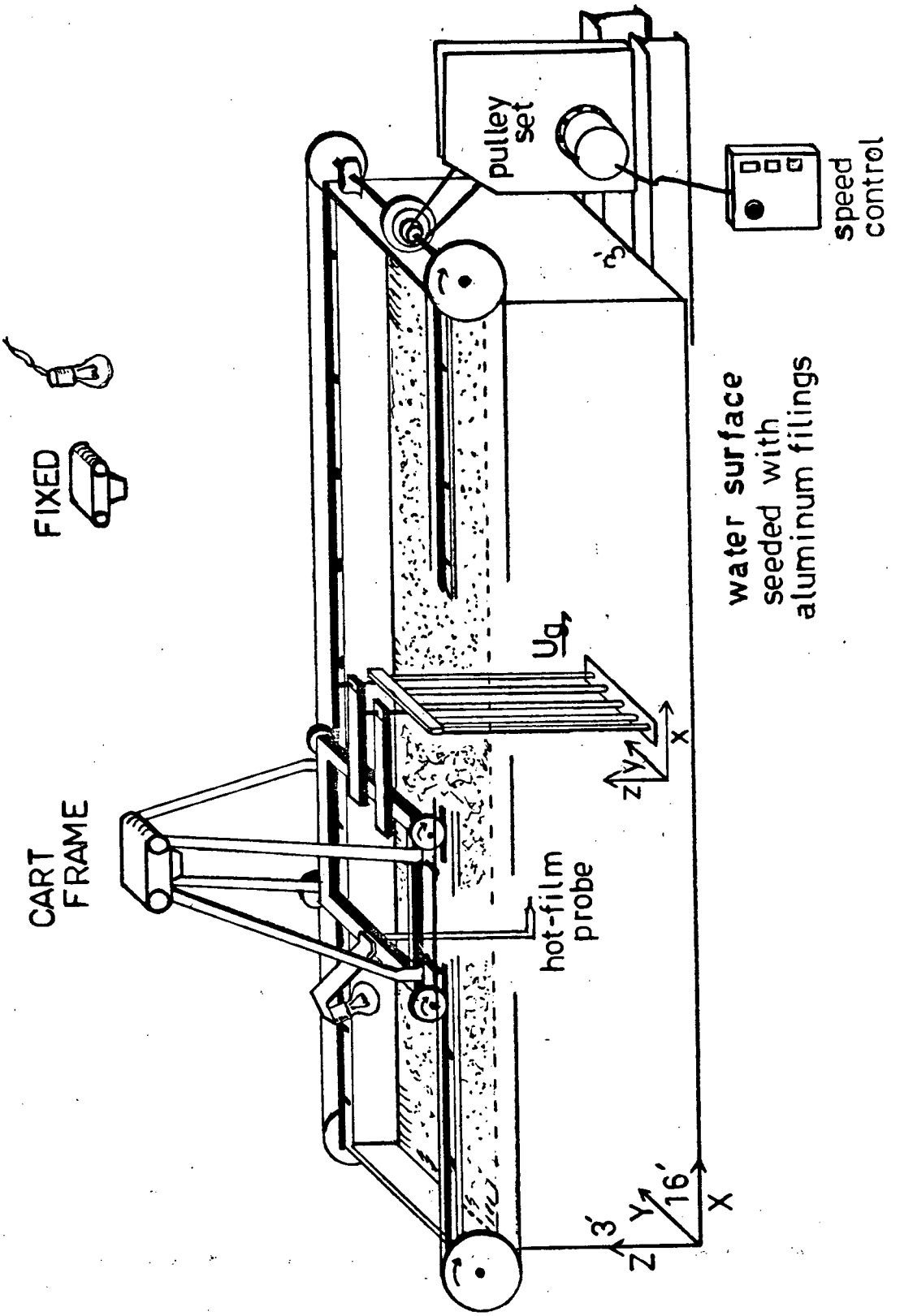

Figure 4 - The Towing Tank

Typically 10 or more runs had to be made to adequately define a power spectrum and it was not possible to obtain hot-film data at distances greater than about 130cm from the generating grid.

3.2 The Tank

A towing tank with inside dimensions of roughly 16'x3'x3' was built for these studies, see figure 4. With a tank of this size one can reach Reynold's numbers up to $1x10^5$ with reasonable sized models and model speeds. The walls were constructed of 3'x4' long panels placed in a welded metal frame. Three of the side panels and one of the floor panels were made of 1/2" clear plastic sheets while the rest were of 3/4" thick plywood. The frame was bolted on top of I-beams resting pn a concrete block foundation which sat inside a plywood catch pan. The catch pan was fitted with float activated marine type bilge pumps in case any untoward leaks or spills occurred. The upper edge of the 16' long sides consisted of an aluminum u-channel on top of which was mounted a 3/4" diameter steel rod. A cart ran over the tank on the steel rods.

The wheels of the cart were equipped with sealed ball-bearings. Rubber o-rings seated about the circumference of the wheels provided some vibration isolation between the cart and the tank. The cart frame was constructed of aluminum angle stock. It was fitted with clamps and sliding bars to secure the objects to be immersed in the fluid. The sliding bars were used to position the models in the tank

and to change the distance between the grid and the hot-film anemometer. An electrical umbilical cable carried the shutter trigger, optical sensor and anemometer signals from the moving cart frame to the instruments in the lab frame. The cart was pulled by two plastic clad steel cables which ran in a continuous loop along the length of each side of the tank. Two 12" pulleys on one end of the tank coupled the cables to the drive shaft. The cables were looped around idler pulleys at the other end of the tank.

The drive system consisted of a two step reduction pulley set with a 4 position step-cone coupling to the drive shaft. The reduction pulleys were chosen to give a final cart speed range from a few centimeters per second to about two meters per second. The drive system was powered by a 1/2 H.P. 90V DC motor with a maximum speed of 1,750 rpm. The motor was operated by a constant speed control box with start, stop, and forward/reverse switches. Two micro-switches, one at each end of the tank, were wired in series with the control box stop button. These switches prevented the cart from inadvertently overshooting either end of the tank. At the 50cm/sec maximum speed used in the experiment the cart took about 30cm to reach cruising speed as well as to come to a complete stop.

Attached to the cart was an optical detector that was used to trigger a timer, figure 5. This detector consisted of an IR photo diode and adjacent photo voltaic cell. It faced a flat black surface about 1/4" away which ran the

length of the tank. White tape was placed at the desired trigger starting and stopping points. When the detector passed over the white tape the photocell would pick up light that was reflected and send a voltage signal to the timer. The timer was started and stopped by the rising part of succesive detector signals. The timer's internal RC clock was calibrated against a frequency counter. The digital counter in the timer box displayed the time between successive trigger pulses. This time and the known distance, ΔX, between the two trigger tabs were used to determine the cart speed. The cart speed thus measured was found to be reproducible to better than 1% over most of the working range of the drive system.

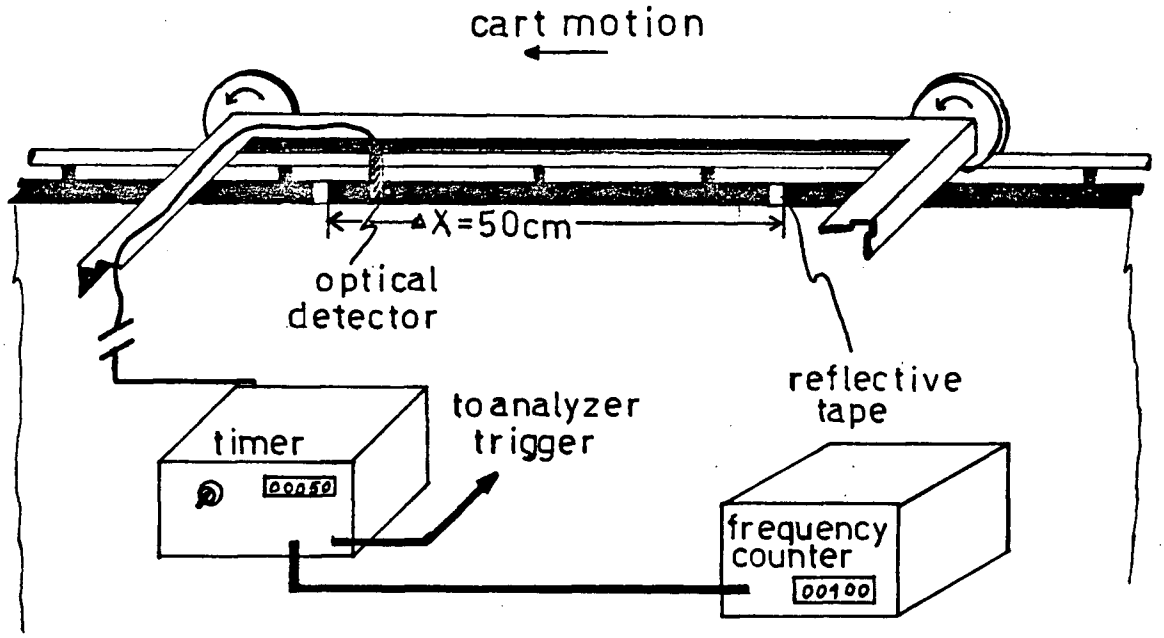

Figure 5 - Optical Detector and Timer

3.3 The Grid

The turbulence was generated by a row of 1/2" diameter round aluminumn bars spaced 2" apart, figure 4. A 1/4x2" end plate was fastened to the bottom of the bars. The grid spanned the tank cross-section with the bars mounted vertically in the Y-Z plane. The grid was expected to produce a turbulent flow that would provide a large sample volume, allow the fluid flow to develop independently of boundary conditions and still allow for a two dimensional analysis.

3.4 Visualization Apparatus

The flow was made visible by photographing the motion of aluminum filings using a Minolta X-570 35mm camera with a 50mm lens and motorized back. A trigger was needed to complete the shutter release circuit on the camera. A conducting flapper attached to but insulated from the cart completed the shutter release circuit when it made contact with an aluminum bracket fixed to the tank, see figure 6. One lead of the shutter release was grounded to the tank through the cart while the other was attached to the flapper. Aluminum brackets were placed at desired locations along the tank. A series of photographs could thus be made by the motorized back equiped camera as the cart moved over the tank. A piece of electical tape on the back side of the flapper ensured photographs were not taken while the cart was returning to its starting position.

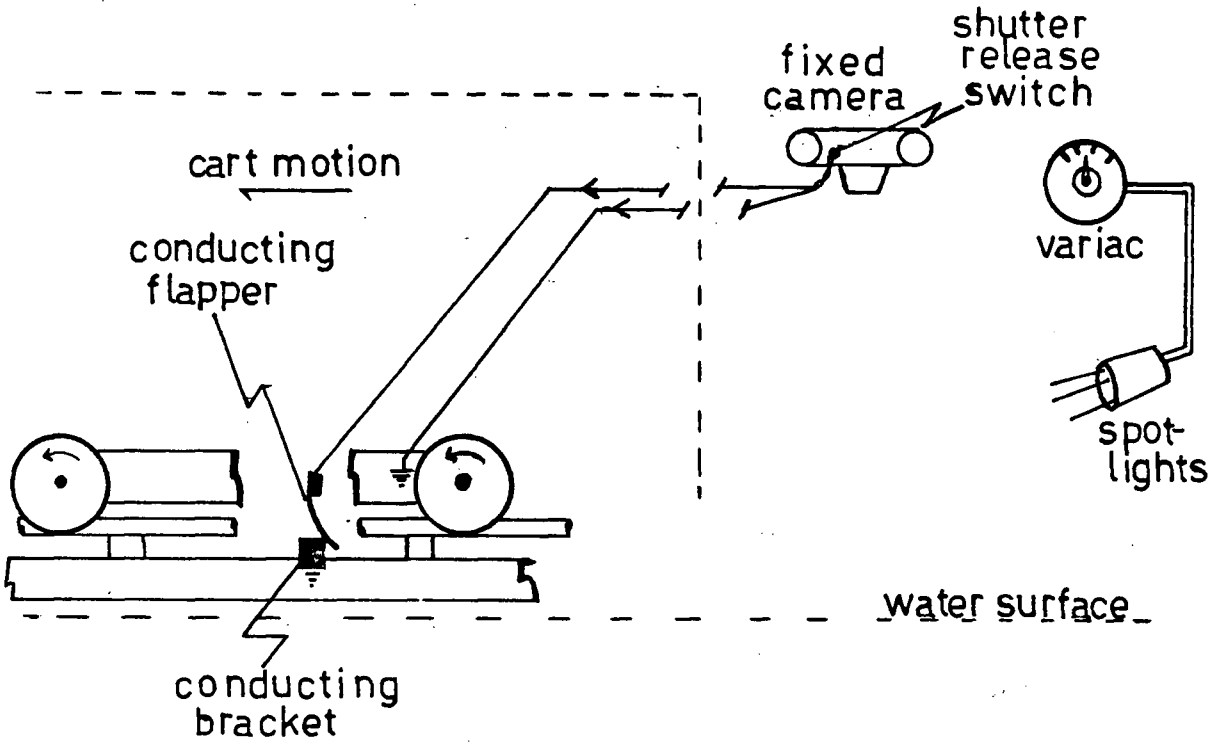

Figure 6 - Lights and Camera Action

Figure 6 also shows the lighting system for the fluid reference frame photography. Four 375 watt spotlights illuminated the surface of the water. The power to these lamps was controlled by a Variac. The lamps were positioned so that no reflections off of the water surface or shadows appeared in the camera's field of view.

The water surface was seeded with aluminum filings of about .1mm diameter which were produced by filing a piece of aluminum above the surface of the water. As the cart dragged the grid through the water the flapper would activate the shutter release. The filing images were recorded on Ilford XP1-400 black and white film which was exposed and developed for an ASA rating of 800. Local

velocities could be obtained by dividing the streak length by the exposure time. Exposure times of 1/2 and 1 second were used for the 20 to 50cm/sec grid speed range.

The flow patterns were studied only at the surface. A neutrally bouyant suspension, required for flow visualization inside the fluid, was not available at the time the experiments were formed. We assumed that the surface of the water provided a sharply defined 'cross-section' of the flow on which aluminum filings were suspended to facilitate the flow visualization. The procedure and results of the photography appears in the next section.

3.5 The Search For Coherent Structures

The preparation for an experiment started with filling the tank. A normal cold water faucet with a 5μm particle filter was used together with an unfiltered hot water tap to fill the tank to a 63+1cm depth. The hot water was added to bring the water temperature to room temperature, 68°F. Without the hot water it would take the initially about 62°F water more than 3 days to equilibriate to room temperature. The 62°F water has about a 10% greater kinematic viscosity.[1] This would result in a 10% lower Reynold's number for a given model size and speed. This is an unacceptable difference.

After the tank was filled a recirculating 5μm particle filter system was used to clear up the inevitably opaque water. Before a run was made the water temperature was

measured. For both the photographic and hot-film measurements the water temperature was within one degree of 68° F. This corresponds to having the kinematic viscosity lie within 0.016×10^{-6} of 1.01×10^{-6} m^2/sec, an ignorable variation.

The first grid turbulence photographs were taken with the camera and illumination system mounted on the cart. It was quickly realized that the coherent structures generated by the grid were likely stationary in the fluid reference frame and would thus be unobservable in the translating frame. Figures 7 show photos in both the grid and lab frame for 30cm/sec grid speeds.

Lab frame exposure times of 1/2 and 1 second were chosen from an intitial test range of 1/60 to 1 second. These resulted in the most easily observable and measureable structures in the flow. The structures were observed as a coherence in curvature of the traces of the aluminum filings. Figures 8 show the filing images for several different exposure times for a 35cm/sec grid speed. The shutter speed which showed the most easily observed and measured coherent structures was found to be 1sec for the 20 and 30 cm/sec grid speeds and 1/2sec for the 40 and 50 cm/sec grid speeds.

---

[1] Eng. Fluid Mech., Roberson/Crowe, HOUGHTON MIFFLIN CO.

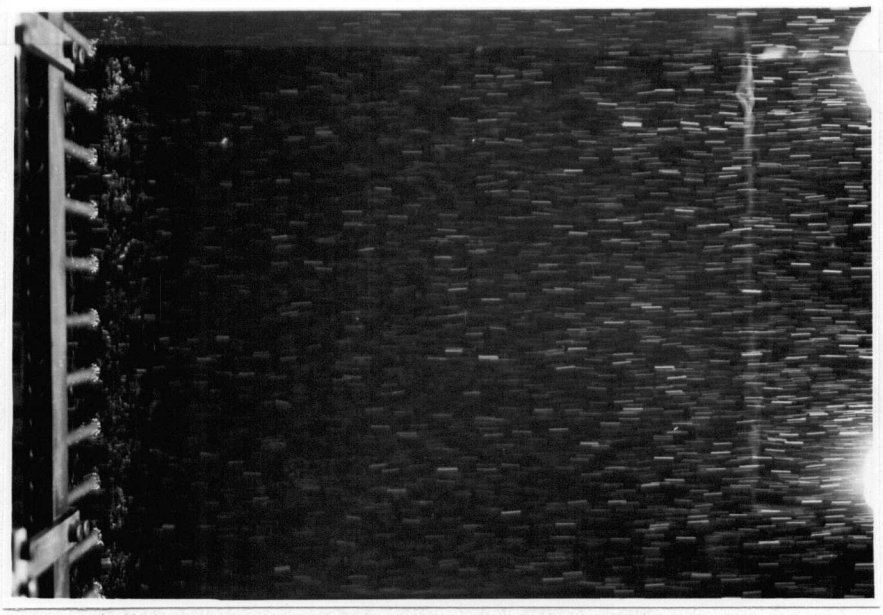

a) Grid Frame 1/15 sec exposure Ug=30 cm/sec

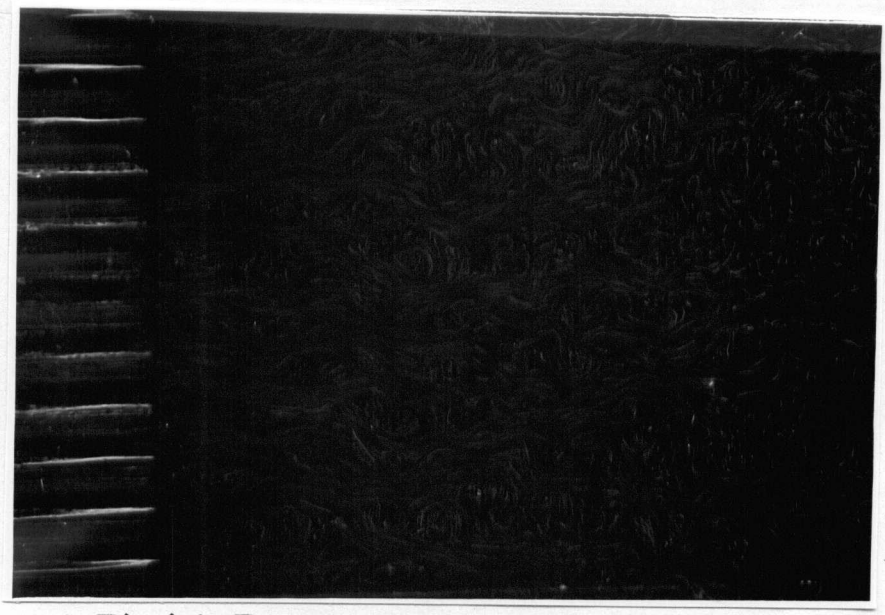

b) Fluid Frame 1 sec exposure Ug=30cm/sec

Figure 7 - Flow Visualization in Grid and Fluid Frames

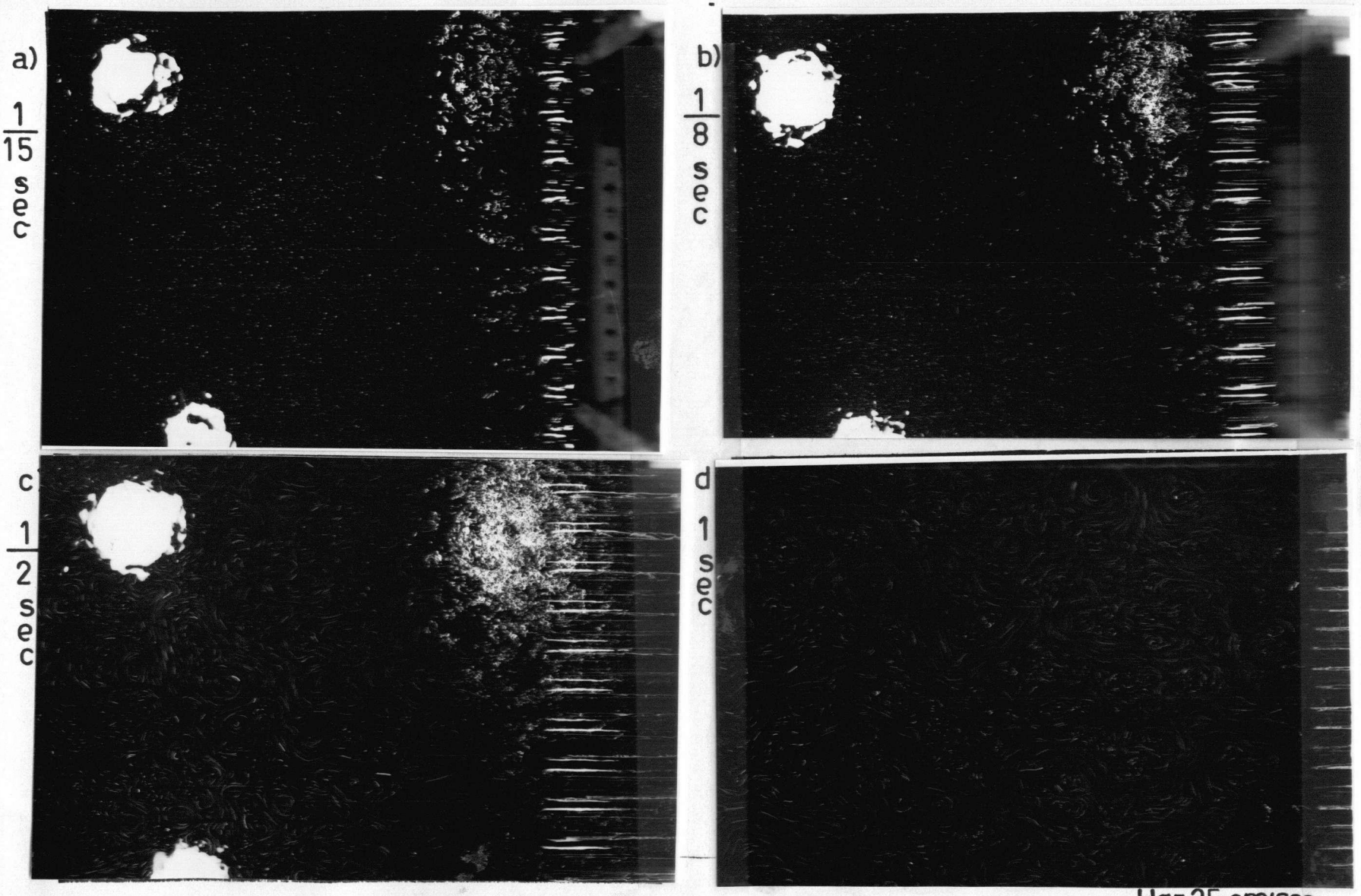

Figure 8 - Visualizations at Different Shutter Speeds

The procedure for obtaining the fluid frame photographs is now explained. The camera was mounted 1.4m above the water surface. This gave a field of view of 60cm in the span direction and 80cm in the longitudinal direction. Pieces of white tape for the timer trigger were placed 50.0 cm apart with the first tab near the edge of the camera's field of view. The cart speed was thus measured during the same time interval as when the grid was creating the flow which was photographed. The shutter release triggers were positioned so that the grid was just leaving the field of view for the first photograph. The other two photographs were taken at times T =50cm/U and T =110cm/U later so that the three shots provided an overlapping time history of the flow beneath the camera. A set of three such photos are shown in figure 9. From the viewpoint of our statistical analysis this is equivalent to a field of observation from x=0. to x=190. cm behind the grid.

Before making any measurements the timer and frequency counter were allowed to warm up for about half an hour or more as the RC oscillator tended to drift when first turned on. The clock was calibrated against the counter to have an oscillating frequency of f =100Hz. This calibration was checked periodically when measurements were made as drifts up to f=0.4Hz occurred over about half an hour.

When changing cart speeds the step-cone pulley which resulted in the highest motor speed for the new cart speed was used. This resulted in a smooth and reproducible cart

motion. Several runs were made to adjust the speed control resistor until the desired cart velocity was reached. This speed setting procedure had the added purpose of mixing the water so that any thermal variations were equilibriated before the measurements began. Aluminum filings were added or replenished as needed. The 40 and 50 cm/sec runs required frequent replenishment as the surface agitation made many of the filings sink to the tank bottom. Once the cart had been returned to its starting position five to twenty minutes were allowed to let the water settle down. At the highest cart speeds the strongly excited surface waves took the longest time to dissipate.

Sets of photographs were obtained for 20, 30, 40, and 50 cm/sec grid speeds. Prints of representative photographs are shown in figures 9 through 12.

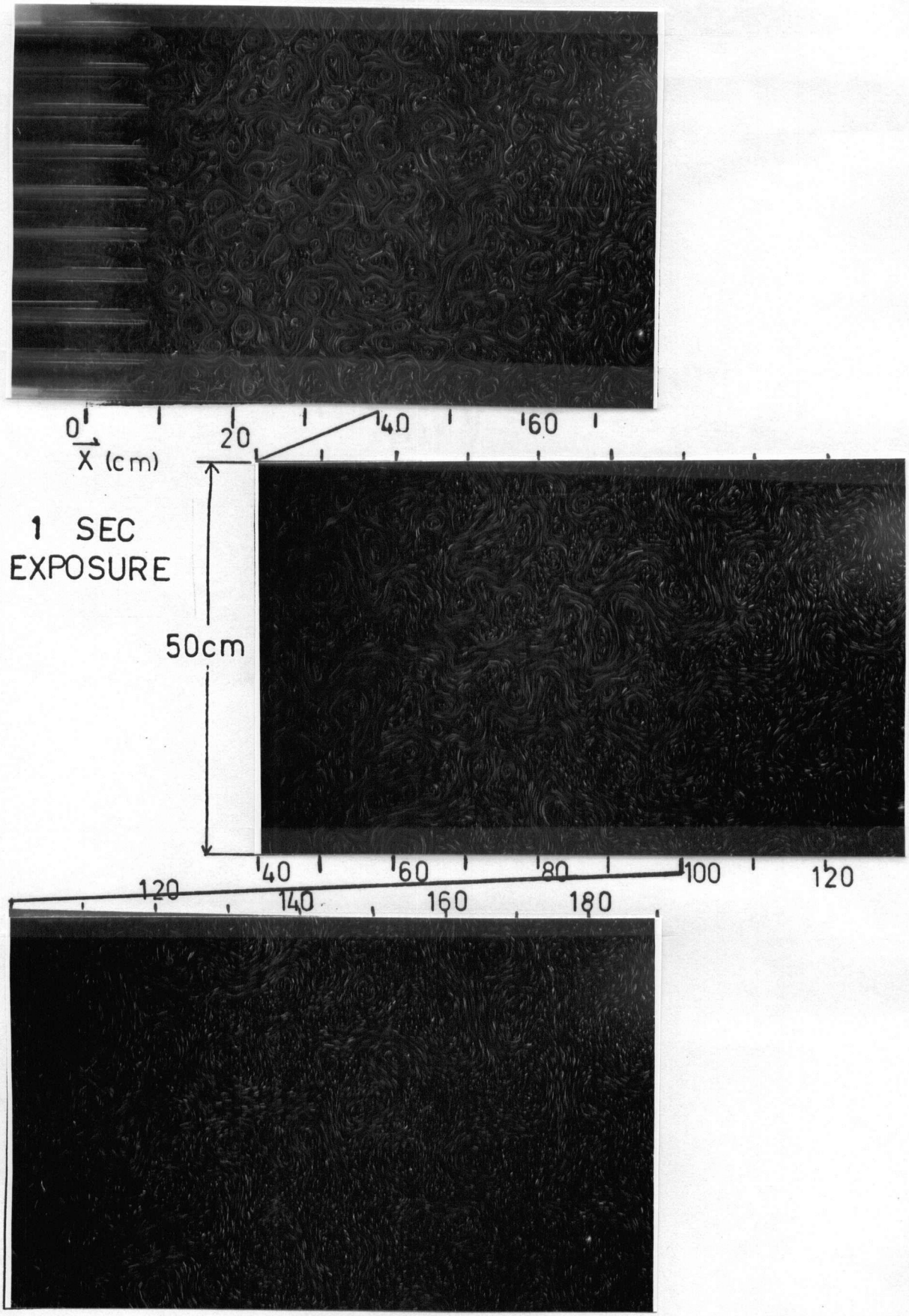

Figure 9 - 20cm/sec Flow Photographs

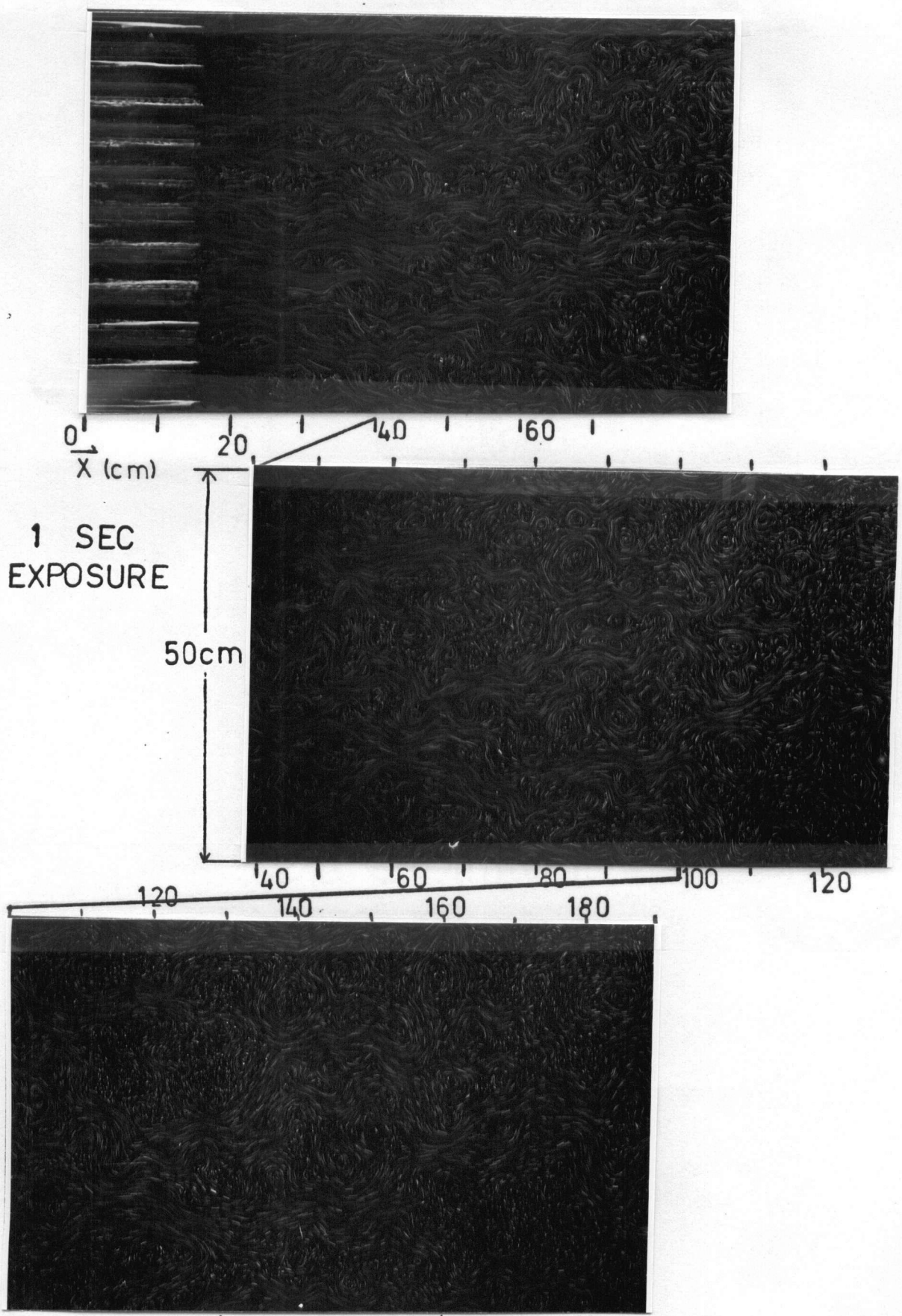

Figure 10 - 30cm/sec Flow Photographs

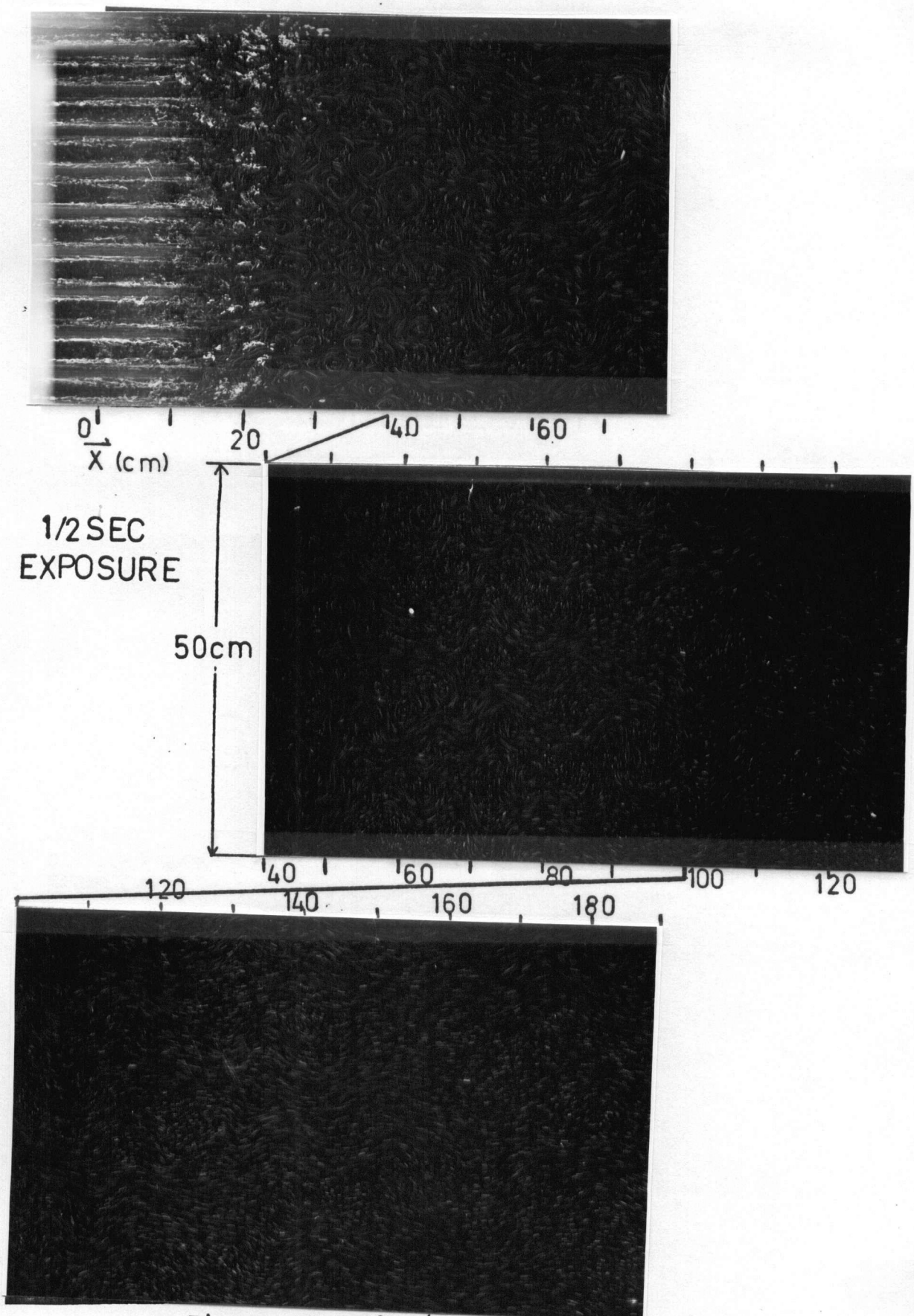

Figure 11 - 40cm/sec Flow Photographs

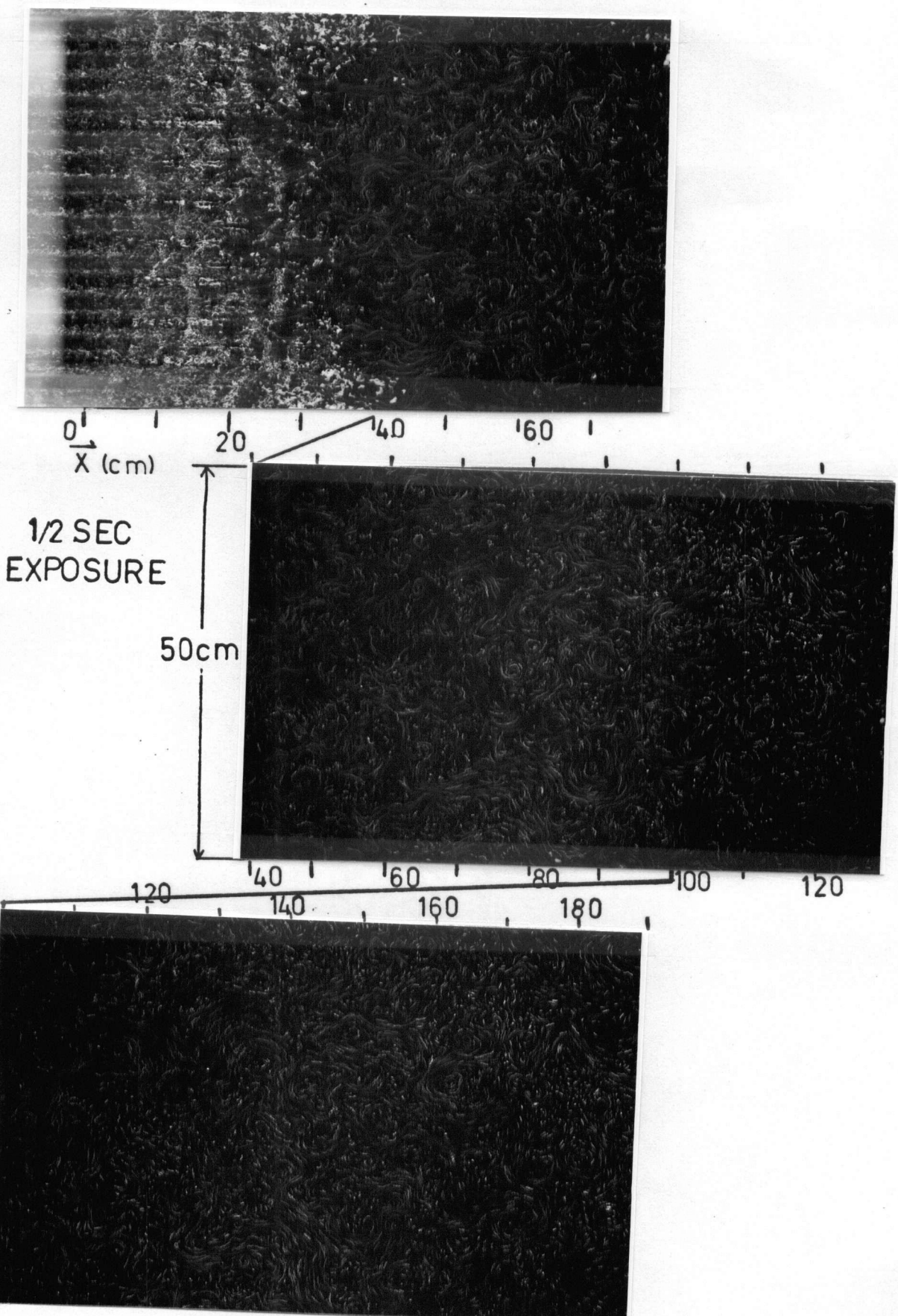

Figure 12 - 50cm/sec Flow Photographs

3.6 Hot-film Apparatus

A Thermal Systems Inc. 1050 CTA (constant temperature anemometer) system[1] was used in conjunction with a Hewlett-Packard HP3582A Spectrum Analyzer to obtain power spectra from the flow field. A flow chart of the diagnostic setup used to obtain the hot-film based power spectra is shown in figure 13.

The hot-film anemometer must be linearized when a new probe type is first used. In addition it must be calibrated before each set of runs. Once set up it generates a signal between 0 and 10 volts which is proportional to the longitudinal flow speed at the hot-film sensor tip. A brief description of the anemometer operation follows.

The hot-film sensor is a thin strip of conducting metal mounted at the tip of the probe. Its resistance depends on the operating temperature T . T is determined by the rate of convective cooling by the flow and the rate of heating by a control current. The control voltage, Ec, at the top of the bridge causes a current to pass through the sensor arm of the bridge. This voltage is controlled to keep the sensor resistance balanced with the control resistance, Rc. The control resistance is set so that the sensor is kept at a resistance slightly higher than its resistance with zero

---

[1] The loan of this equipment from Dr.Quick of the UBC Engineering Dept. is gratefully acknowledged.

control voltage. This holds the sensor element temperature above that of the surrounding fluid as the sensor resistance increases monotonically with temperature. The sensor's thermal energy loss rate is a unique function of the fluid flow rate past the sensor for constant water density and temperature. The voltage, Ec, required to maintain the sensor at a constant temperature is thus a unique function of the flow velocity at the sensor tip.

The linearizer unit is used to convert this voltage signal from this non-linear function of the flow velocity to one which is. The linearized signal is then fed into the signal conditioner which was used to remove fluctuating components lower than 2 Hz and greater than 1 kHz in frequency.

When the largest velocity fluctuations are much less than the convection velocity the fluctuating part of the output signal is simply due to the longitudinal component of the fluctuating velocity, see Appendix A. The wedge shape of the probe is designed to further suppress the contributions to cooling from lateral components of the flow.

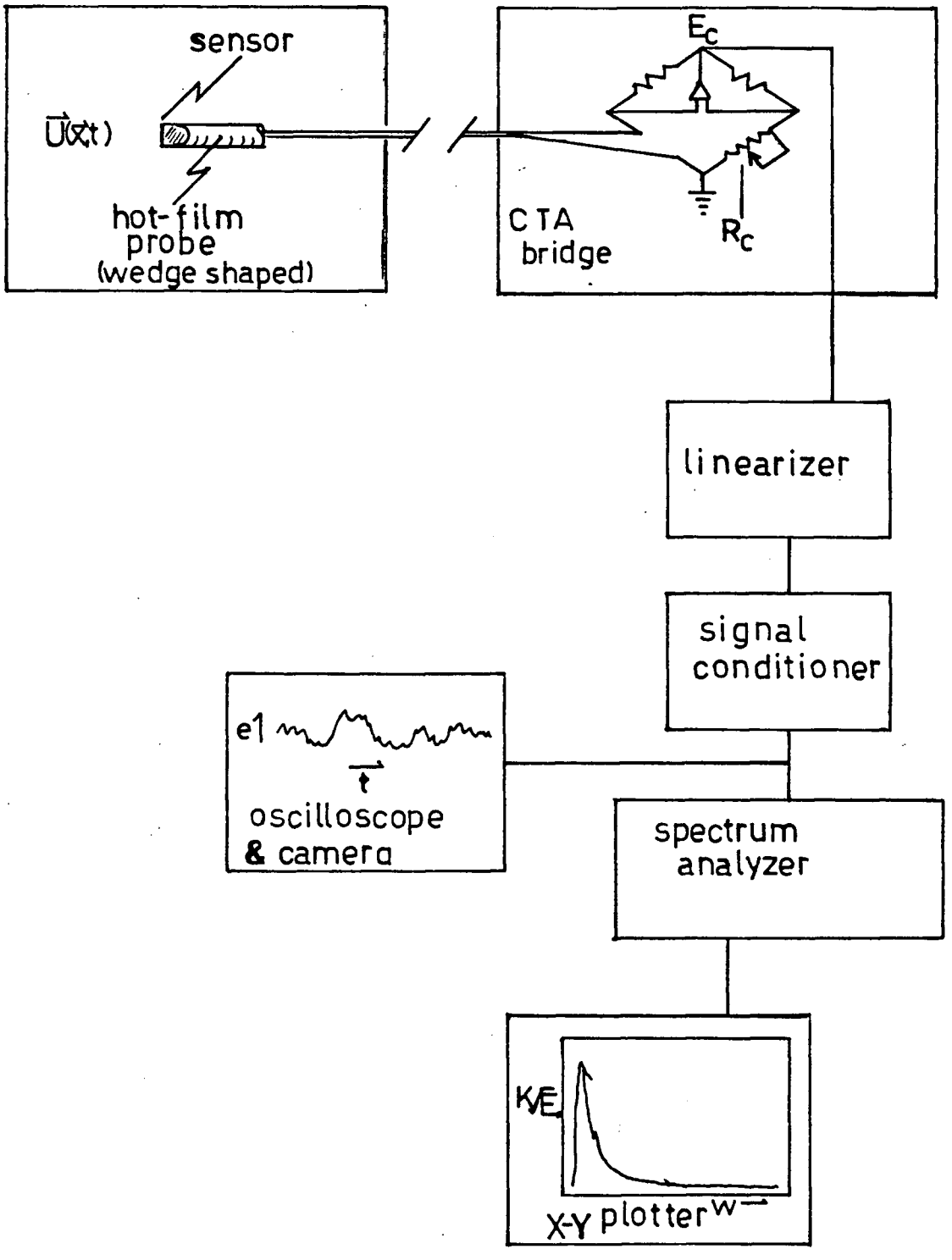

Figure 13 - Hot-Film Power Spectrum Schematic

The linearized and filtered signal is displayed on the Tektronics 454A oscilloscope and fed into the spectrum analyzer. A Tektronics C-31 polaroid camera was used to obtain some typical photos of the fluctuating voltage trace. The spectrum analyzer had an external trigger input which could be used to start the sampling time interval, of time duration Ts=2.5sec for the 100Hz frequency span. This feature was used to ensure data was taken only when the hot-film probe was in the turbulent flow field. The timer's trigger was used to trigger the spectrum analyzer data loading. If the analyzer was ready for a new data loading sequence a new time record would start when the optical detector next encountered a piece of white tape. Tape was thus placed at strategic positions along the tank. The first two pieces of tape were placed X=50.0cm apart. These triggered both the timer and the analyzer. Subsequent signals from the optical detector were only used by the analyzer. The analyzer trigger had to be disconnected before the cart was returned to the starting position or meaningless spectra would be added to the previous data. When a sufficient number of spectra, typically 20, were averaged the resultant power spectrum was plotted using an HP x-y plotter which interfaced to the spectrum analyzer. This hardcopy was then digitized for subsequent analysis using facilities at the UBC computing center. The next section gives a detailed account of how the hot-film data was obtained.

3.7 Hot-film Power Spectra

In preparation for the hot-film experiments the tank was filled and filtered as for the photography work. It was even more important that the water be clean and have a constant temperature for the hot-film measurements than it was for the flow visualization. The sensor cooling rate was very sensitive to both temperature variations and dirt. Before any anemometer measurements could be taken the linearizer had to be set up for the 1232W model hot-film probe. The instructions in the TSI "MODEL 1050/1050A Constant Temperature Anemometer" instruction manual were closely followed. Only the basic setup procedure will be described here. The probe arm of the bridge consisted of a 30' coaxial cable with probe mount, together having resistance Rcab, and the probe itself, resistance less sensor element Rp, at the tip of which was the sensor element, resistance Rs, see figure 13. It was first necessary to measure the unheated sensor resistance, Rs, and multiply by the overheat ratio of 1.06 to obtain the sensor operating resistance, Rop. The probe support plus cable resistance, Rcab, was measured by nulling the bridge with a shorting wire in place of the probe. This was done by balancing the probe arm against a variable decade resistance, Rc, which formed the opposite bridge arm. The probe minus sensor's resistance, Rp, is then added to the decade resistance and the decade resistance balanced against the ZERO OHMS resistor. The ZERO OHMS resistor thus

adjusted to the probe arm minus sensor resistance, Rcab+Rp, is connected in series with the decade resistor. The decade resistance would therefore read only the sensor resistance, Rs ,when the bridge was balanced with the probe in place. The probe could now be inserted into the probe support and immersed in the 68 F quiescent water. The unheated sensor resistance, Rs, was read off the nulled bridge and the operating resistance determined, Rop=Rsxoverheat ratio. The operating resistance, Rop, was dialed into the decade resistance, Rc. When the bridge control circuit was switched to RUN the sensor would be maintained at the elevated temperature. For the data presented in this thesis the sensor resistance Rs of 3.92 ohms multiplied by the overheat ratio of 1.06 determined the operating resistance Rop to be 4.15 ohms.

The 1050 anemometer provided a choice of three different control bridges. The bridge used depends on the power requirement determined by the probe type and flow environment. The number 1 bridge is generally used for low power requirement applications such as probes in air or small probes in water. The number 2 bridge was used for the hot-film probe as its higher output current was needed to avoid the voltage clipping which was observed when the number 1 bridge was used.

After the bridge was set up a calibration curve of bridge voltage, Ec, versus flow speed was measured, figure 14a. This non-linear curve was needed to adjust the

linearizer settings. It was obtained by measuring the bridge output voltage using a digital volt meter while the cart moved the probe through the water at a known speed. For these measurements the grid was removed so that the fluctuation levels were very low. The probe was positioned about 7.5cm beneath the water surface and was aligned parallel to the direction of the cart's motion. The cart speed was measured using the timer.

The bridge signal was linearized by a rather tedious process of setting 9 interdependent slope changing resistors on the model 1055 linearizer. The bridge voltages corresponding to zero and the maximum flow speed of interest were supplied to the linearizer and the linearizer ZERO and SPAN controls were adjusted so that the linearizer would output corresponding voltages of 0.00 and 10.00 volts. The available linearizer had a broken resistor for its 4th slope point. A reasonable linearization could only be achieved with the resistor turned completely clockwise. A slight variation from this position produced a discontinuous change in the linearizer's response. The linearized curve appears over the calibration curve in figure 14. Subsequent linearization checks were made during and after the experimental runs. The calibration constant is determined as the slope of the linearized curve. Minor variations of this slope in the 40cm/sec region were observed and so the average value of the three calibrations was used..

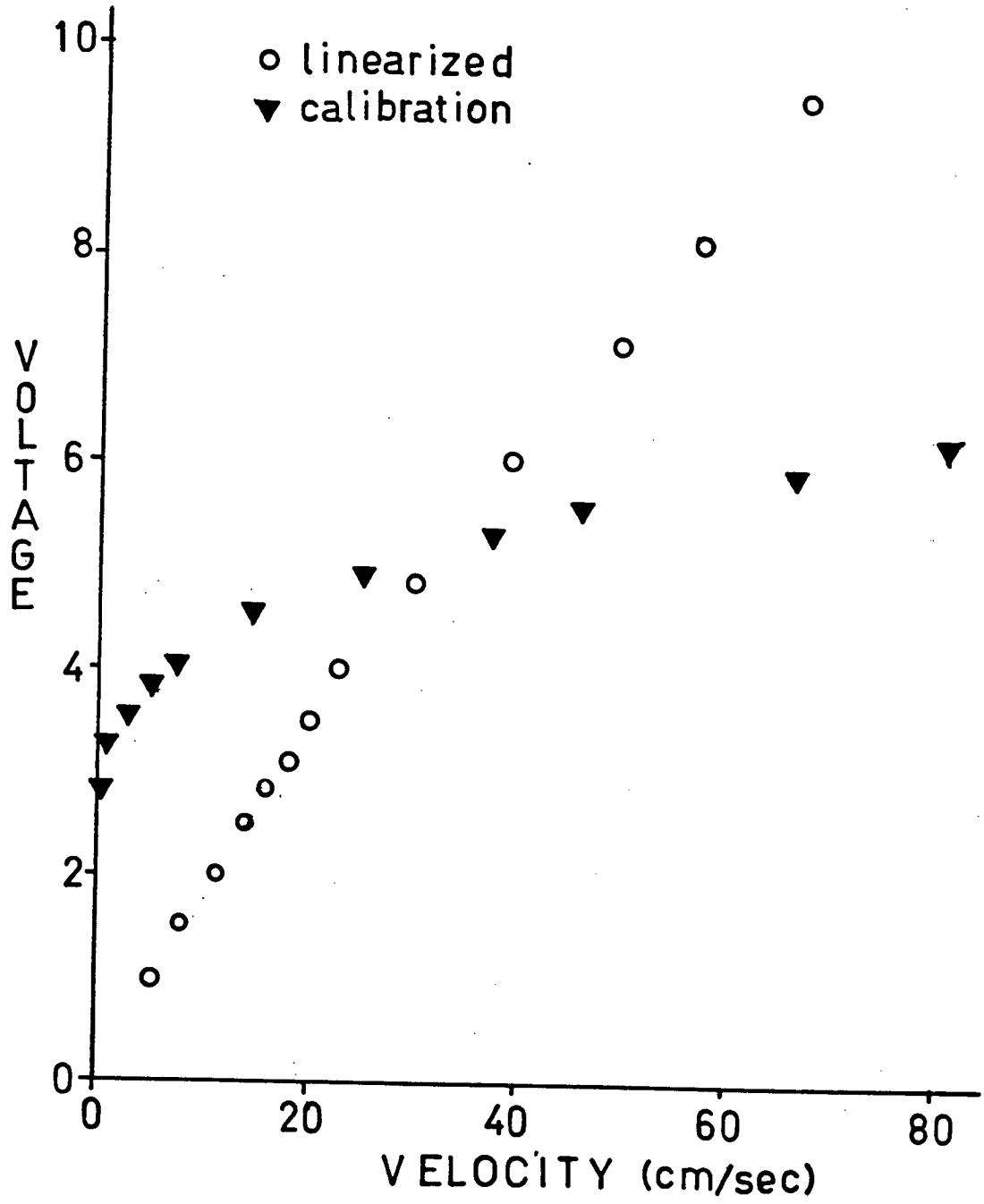

Figure 14 - Hot-Film Linearization

The linearized signal was fed through the signal conditioner with a pass band of from 2hz to 1Khz and then to the monitor scope and spectrum analyzer. Some oscillograms of the linearized fluctuating anemometer signal appear in figure 15.

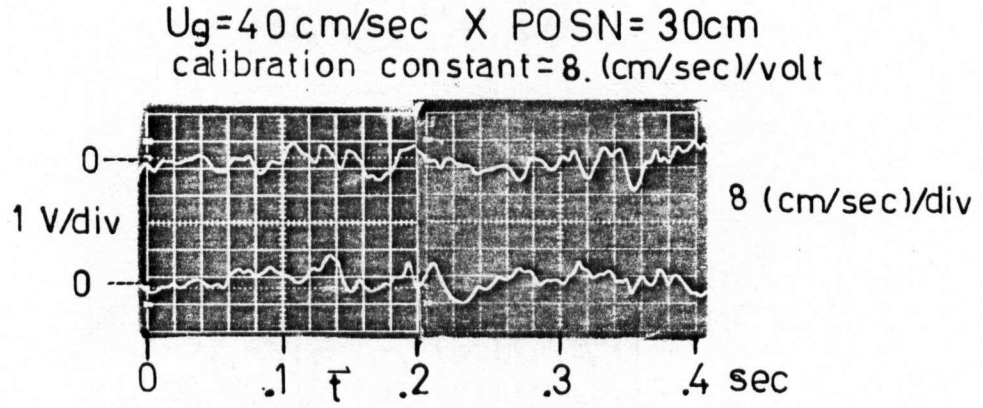

Figure 15 - Hot-Film Oscillograms

The HP3582A Spectrum Analyzer was used to obtain power spectra from the fluctuating anemometer signal using the following control settings. The input switch was in the "chassis isolated" position. The DC coupling mode was used as the signal conditioner had already filtered the signal. This coupling ensured that no more of the low frequency end of the signal was filtered. The input section had an input sensitivity selector which was set at the most sensitive position possible while still not having the data overload indicator light up. The higher turbulence intensities required a lower input sensitivity. The frequency span was chosen to be from 0 to 100Hz. Preliminary measurements showed no significant energy content at frequency greater

than 100Hz for the grid speed range used in these experiments. The analyzer had a choice of three band pass shapes depending on whether amplitude or frequency resolution was desired. The Hanning band pass shape was used as a compromise between the two extremes. RMS averaging was selected so the analyzer would average successive power spectra and the data loading trigger section was set up to load data on the external trigger signal supplied by the timer.

After the analyzer, hot-film probe to grid separation, and the cart speed were set up the cart was moved to its starting position. Enough time was given for the water motions to subside. The spectra averaging was reset and the timer's trigger output was connected to the analyzer's data loading trigger input. The drive motor was started and the cart towed the grid and hot-film probe through the water. The timer box clocked the 50.0cm distance and also triggered from one to four analyzer sampling periods. This number depended on the cart speed as the data loading took a fixed amount of time, Ts=2.5sec. After the cart stopped at the end of the tank the timer trigger was disconected and the cart returned to its starting position. Depending on the cart speed, from five to about twenty minutes elapsed before the waves in the tank died down and another run was made. It was found that the hot-film probe mounting had a mechanical resonance which showed up in the power spectra. The mounting system was reinforced and the resonance

diminished in amplitude and slightly increased in frequency. To distinguish between turbulent signals and this mechanical resonance a power spectrum was obtained with the water quiescent. This spectrum appears in figure 16. Hard copy of the power spectra were obtained from the spectrum analyzer using an HP X-Y plotter. These plots were then digitized and stored in computer files for susequent analysis. When the spectra were digitized the probe support resonance contribution was ignored. A typical X-Y plot is shown in figure 17. The digitized curve has been drawn through the spectrum.

Power spectra were obtained for various grid speeds and probe-grid separations. The distance of the probe from the grid was changed by sliding the grid in its mounting brackets. The experimental conditions were chosen so that the hot-film power spectra would correspond to those predicted from the flow visualization photographs.

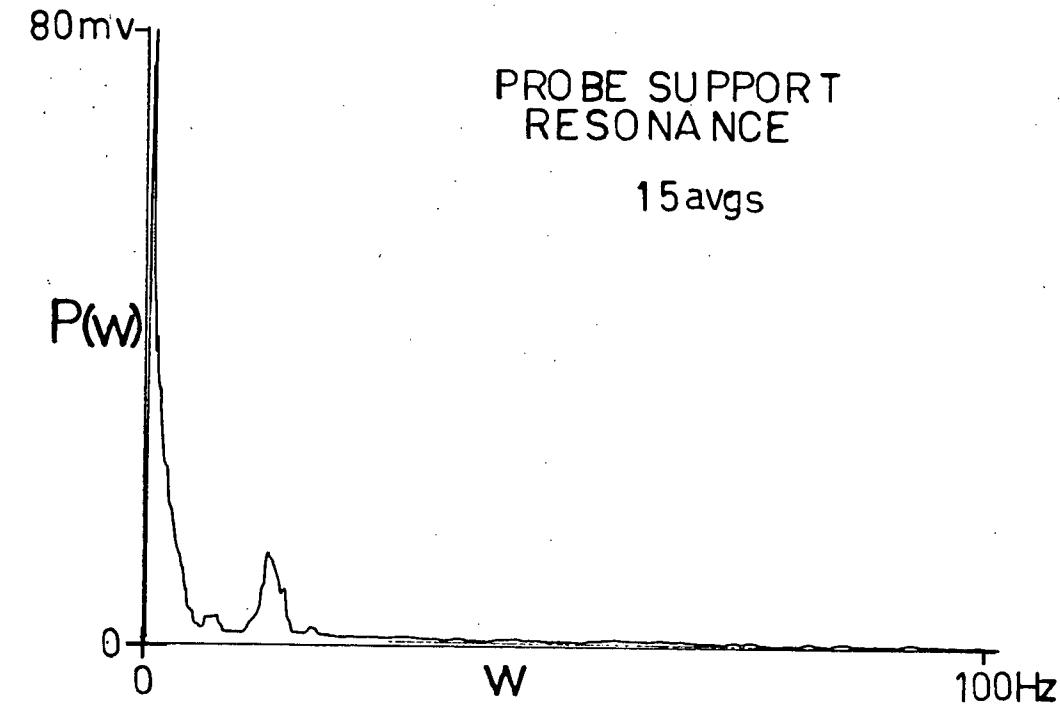

Figure 16 - Probe Support Resonance

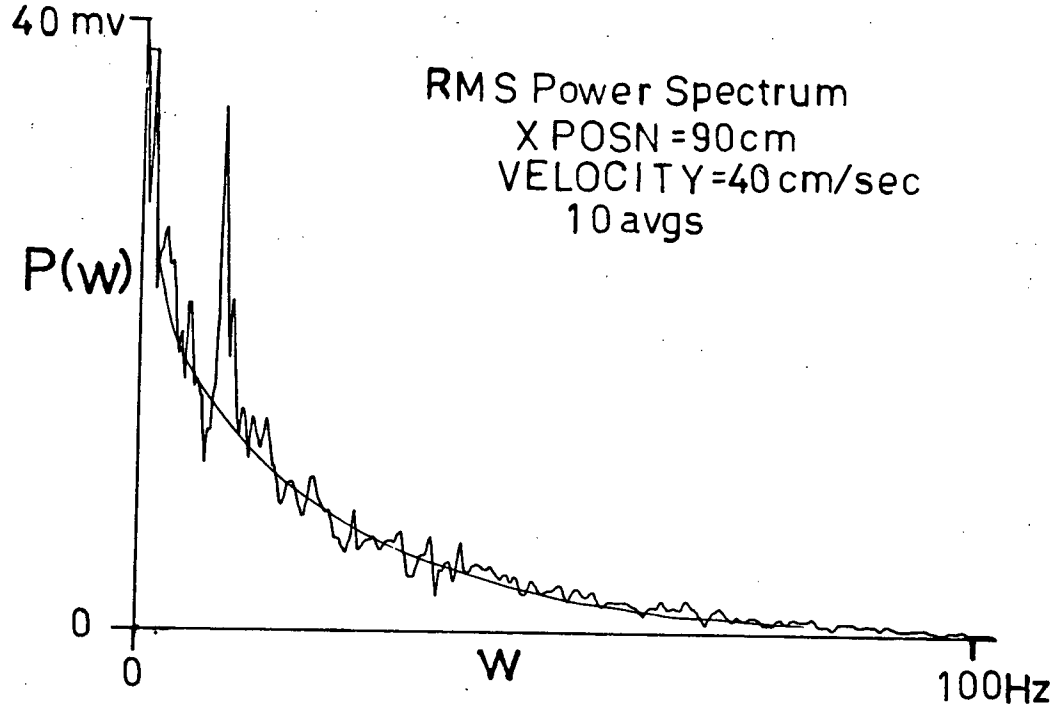

Figure 17 - Typical Analyzer X-Y Plot

IV. EDDY-SIZE DISTRIBUTIONS AND HOT-FILM SPECTRA

4.1 Introduction

A major aim of this thesis is to compare the eddy-size spectrum with the statistical description of turbulent fluctuations. This was seen as a test for the validity and viability of using coherent structures to model turbulence. A personal aim of the author was to learn how the statistical description is used to describe turbulent flows.

Figure 18 is a flow chart of the analysis used to compare the two descriptions. To obtain the eddy-spectra the flow visualization photos were analyzed in terms of the coherent structures. The eddy-size distribution is then used in a computer code to predict the power spectral density. Assumptions about the distributions of the eddies in space and their convection velocity were needed to generate a time record of the longitudinal velocity fluctuation. The computer code analyzes the time record in a manner nearly identical to that used by the spectrum analyzer in the hot-film experiment. The prediction of power spectra from the eddy size distributions and the assumptions used are described in section 4.3. Section 4.4 describes how power spectra were obtained from the anemometer signal. The power spectra were compared and used to obtain the integral length scale and total fluctuating kinetic energy. The results of this analysis are presented and described in the last section of this chapter.

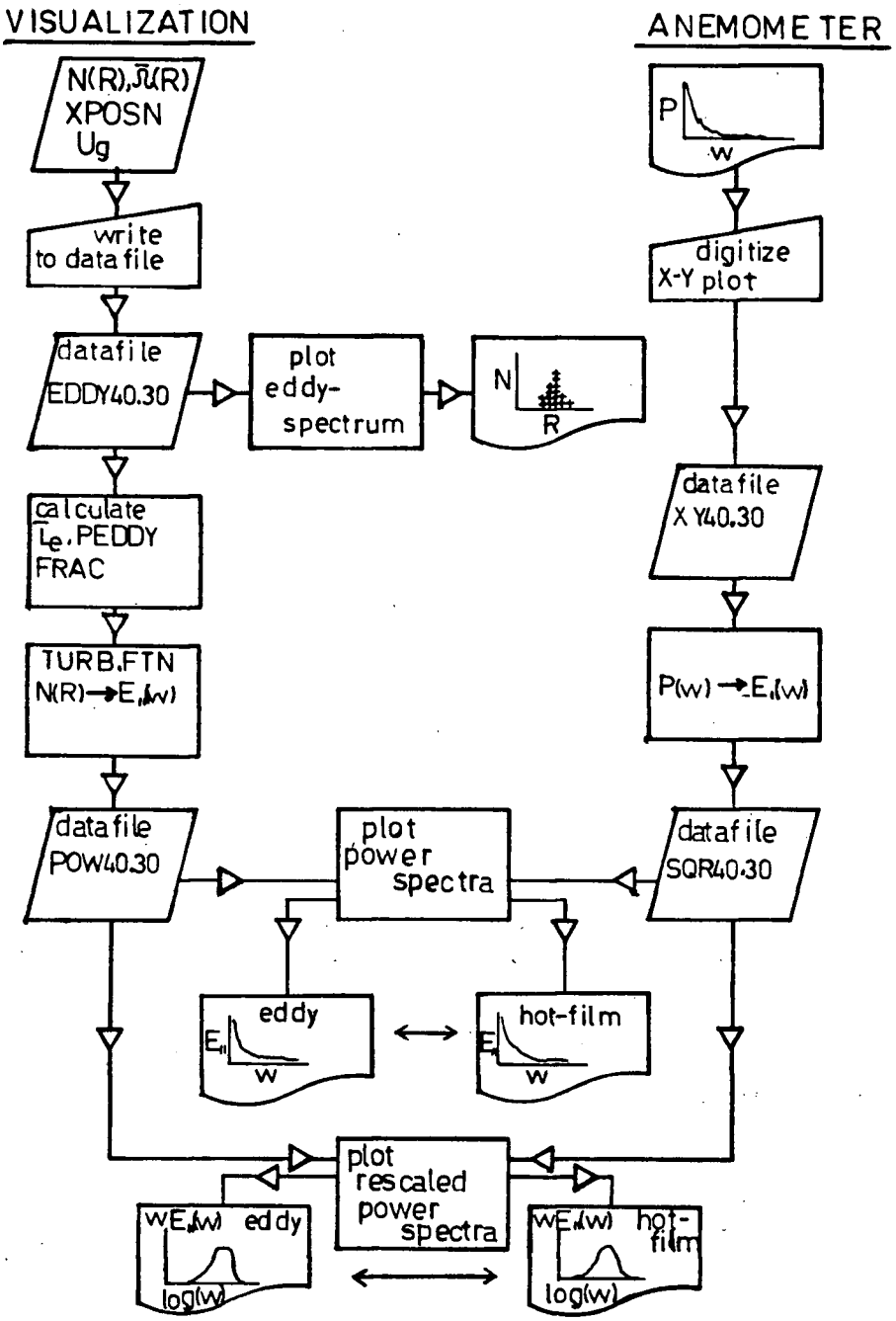

Figure 18 - Power Spectra Comparison

4.2 Eddy-Size Spectra

Eddy-size spectra were obtained from the photographs of the flow patterns as follows. The flow patterns on the negatives were projected onto a sheet of white paper to half their original size. This paper was divided into 10cmFS (full scale) wide bins, see figure 19a. The distance label, Lb, corresponds to the distance between the middle of the sampling bin to the average position of the grid during the exposure time. The bins could equally well have been referenced by the average time since the grid had passed by. This time, Tb, would simply be the bin distance Lb divided by the grid speed Ug.

The person analyzing the flow patterns drew the outline of what he considered to be the coherent structures on the paper. This process is of course highly subjective. The 40cm/sec photos were analysed by a person who had little indoctrination as to what a coherent structure should look like. Generally we assumed that the periphery of the structure should be the largest closed streamlines. Figure 19a also shows the structures circled. This analysis is very crude although, as it turns out, it was both quick and yields useable eddy spectra. An automated decomposition of the flow field according to rigorously defined criteria was beyond the scope of this thesis. We decided to learn from the consequences of our simple analysis.

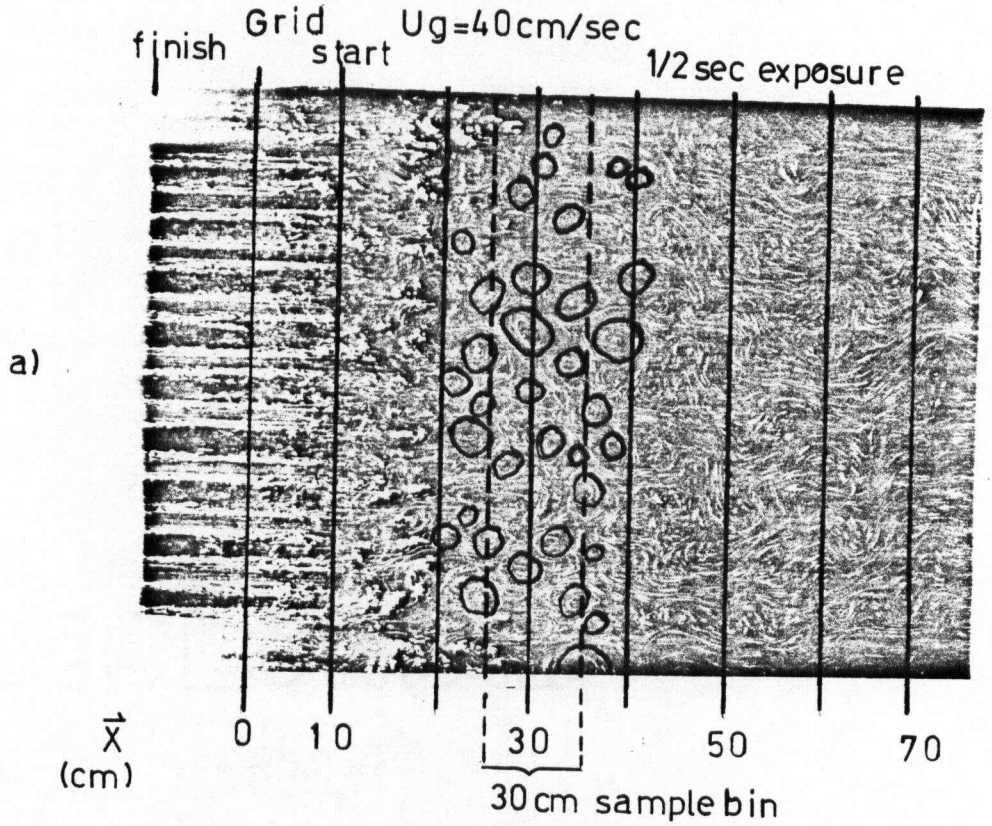

Figure 19 - Eddy Analysis

Having outlined the contours of the eddies a circle template was used to determine their radii. Non-circular structures were treated as circular eddies having the same area. Eddy radii were estimated with an uncertainty of 1mm. For each bin the eddy size distribution, N(R), was recorded after the radii had been determined, figure 19b. The sum of the eddy distributions from all ten sets of photographs for one flow speed provided a statistically significant distribution, figure 19c.

The eddy's internal angular velocities were measured using a clear plastic angle template. The template was centered over the structure and the angle that a trace made with respect to the center of the structure was conveniently read off the angle scale. The results of these measurements for the 40cm/sec data appear in figure 20a. This measurement proved much more difficult and uncertain than estimating an eddy size as the images often did not have a cicularly symmetric velocity distribution. Also the low trace densities needed to avoid trace overlapping made characterization of an eddy's angular velocity distribution very difficult. It was thus necessary to make some assumption about the velocity profile within an eddy. We choose a rigid body rotation, no internal stress, for the velocity profile. This choice was made on the basis of observation and convenience.

The assumption that the eddies undergo rigid body motion was reasonably consistent with observation.

The eddy-size spectra for ten sets of photographs for a particular cart speed were summed. These spectra and the average eddy angular velocity as afunction of distance were written into a computer file. The population at a given radius was averaged with the populations of the eddies one size greater and one size smaller to remove a possible analysis bias in using the circle template. The smoothed eddy-size spectra summed over all ten sets of photos for the 30 and 40cm/sec cart speed appears in figures 21 and 22. A qualitative discussion of these spectra is presented in the discussion section at the end of this chapter.

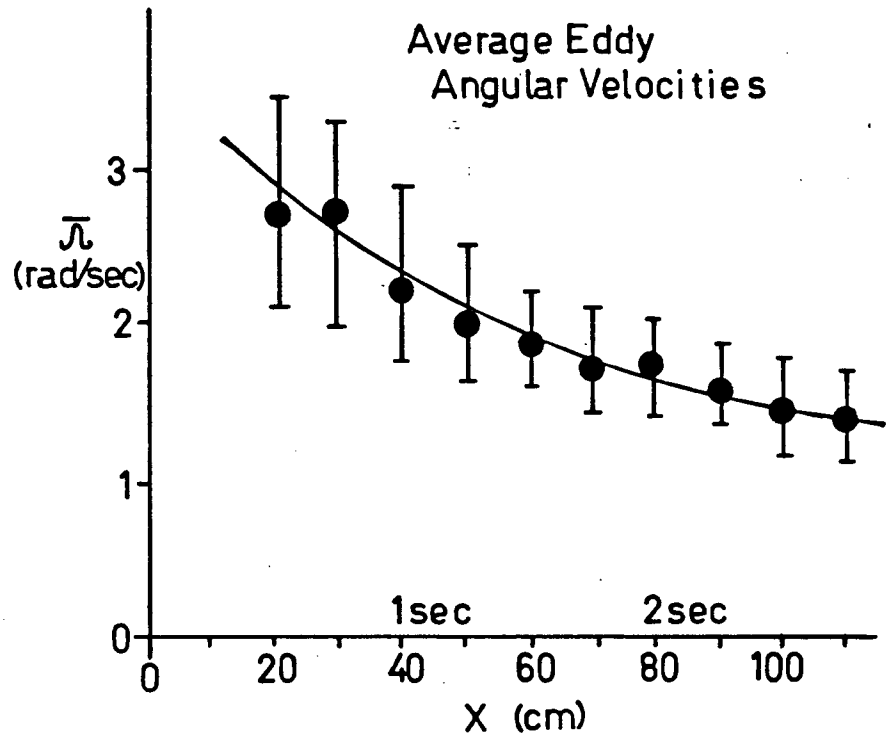

Figure 20 - Eddy Angular Velocities

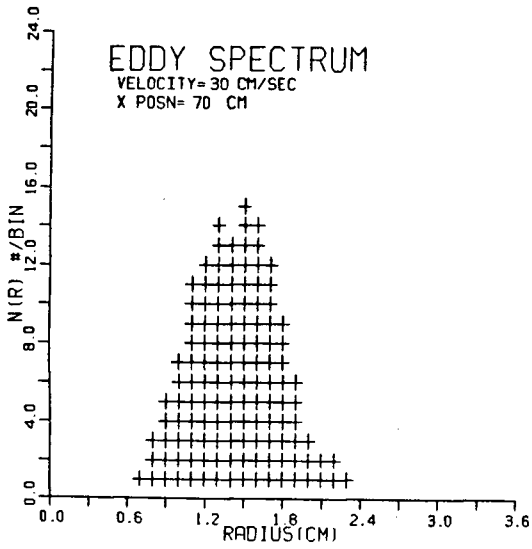

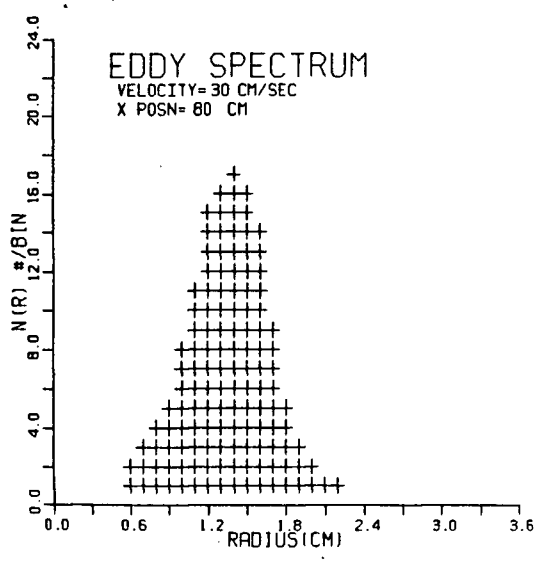

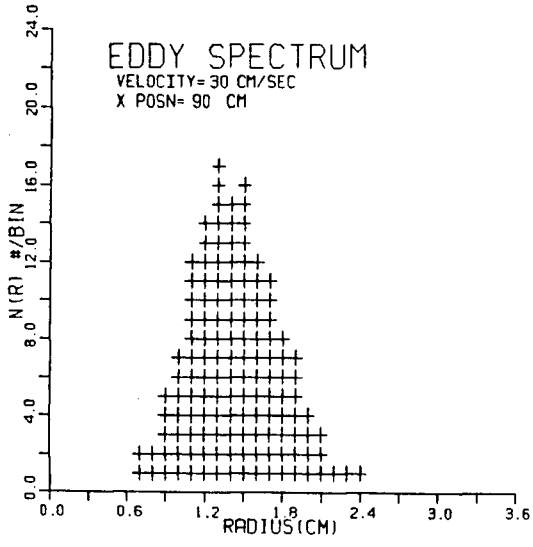

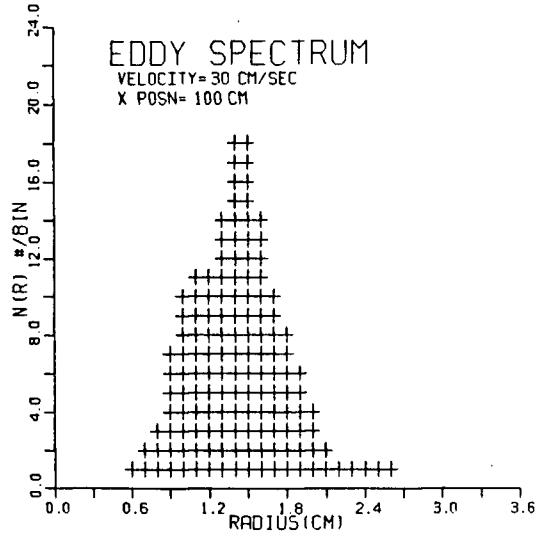

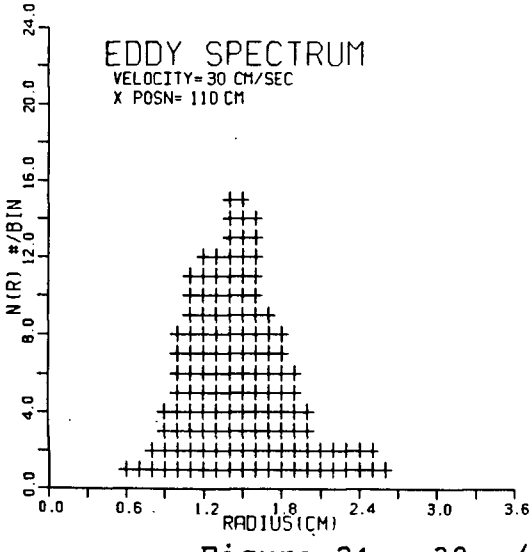

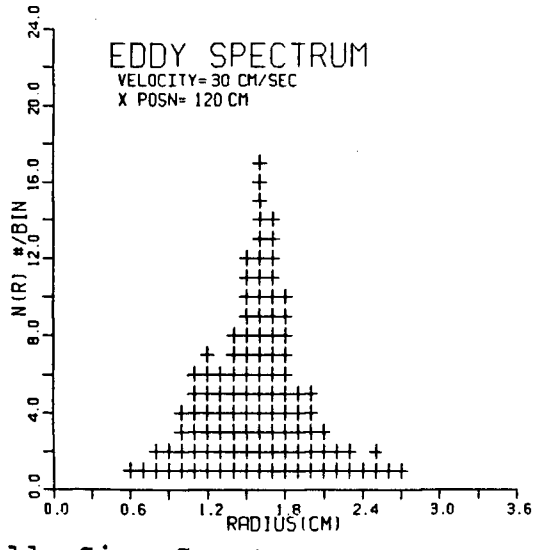

Figure 21 - 30cm/sec Eddy-Size Spectra

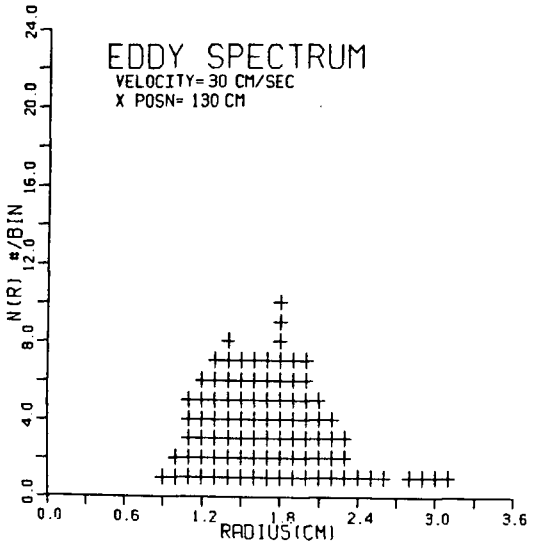

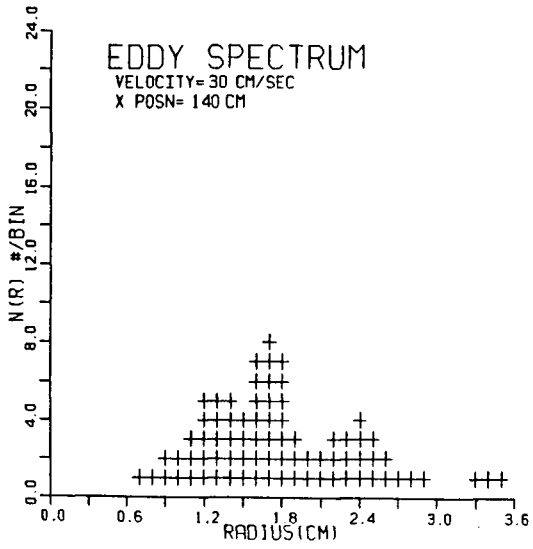

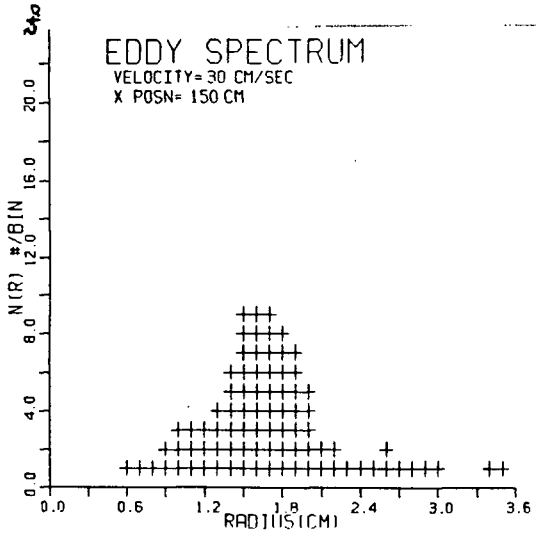

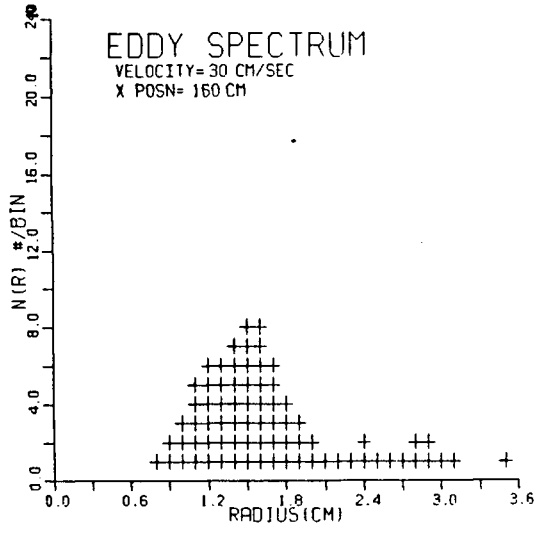

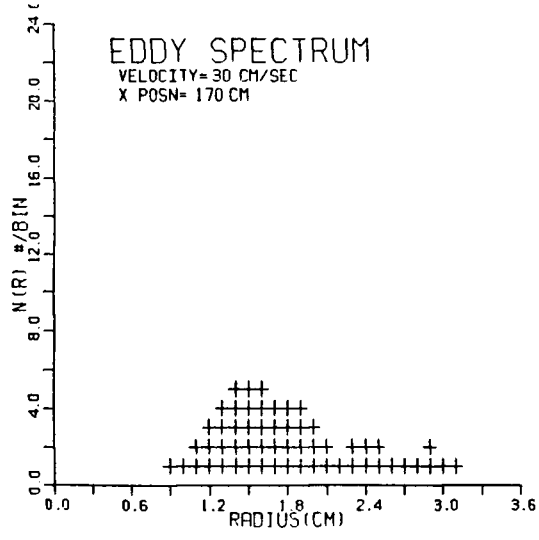

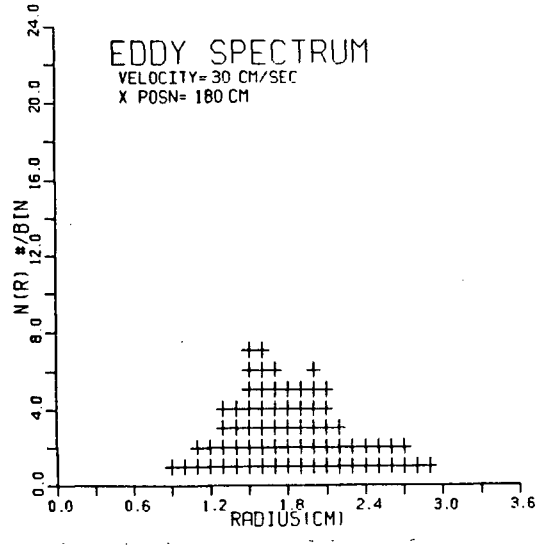

Figure 21b- 30cm/sec Eddy-Size Spectra

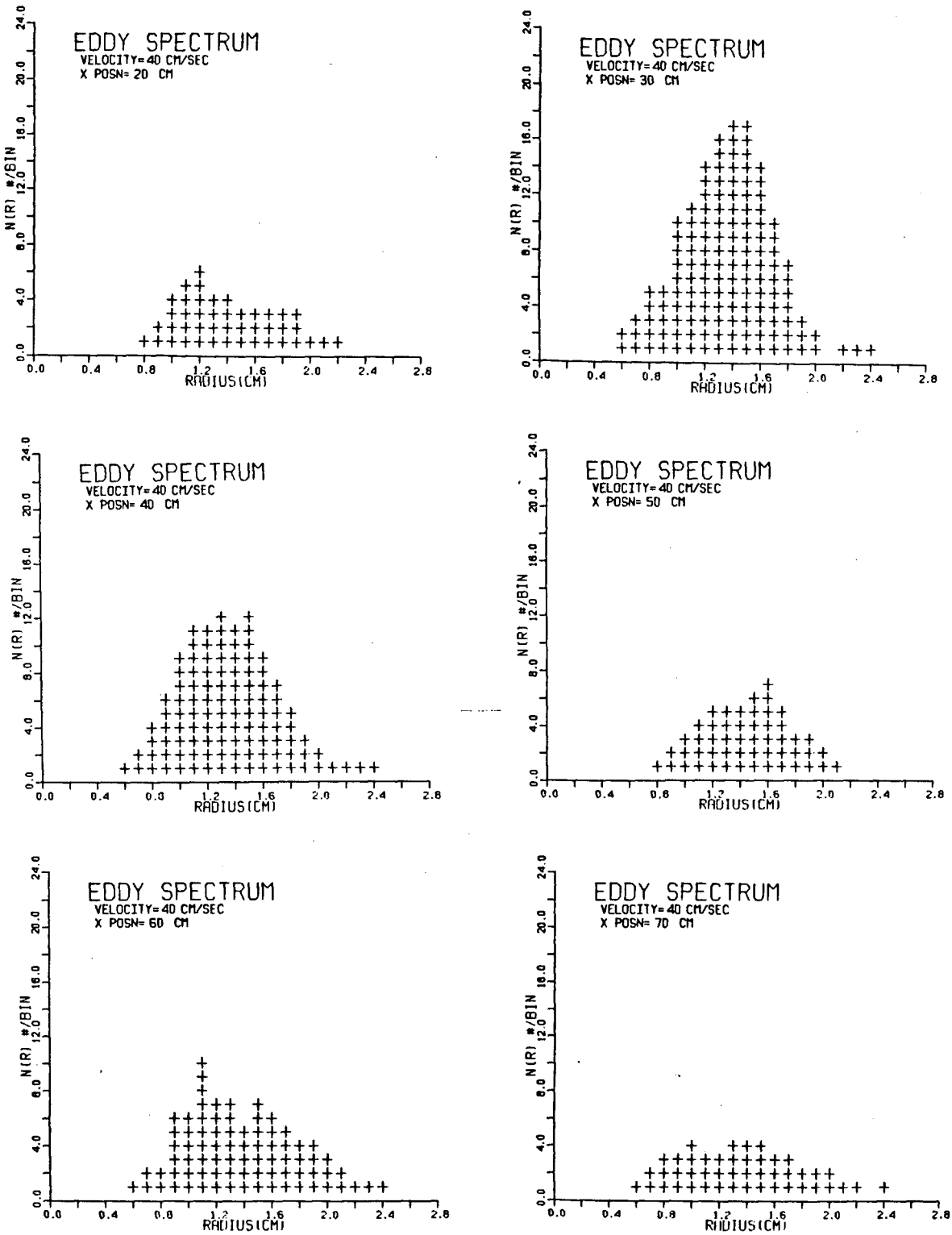

Figure 22 - 40cm/sec Eddy-Size Spectra

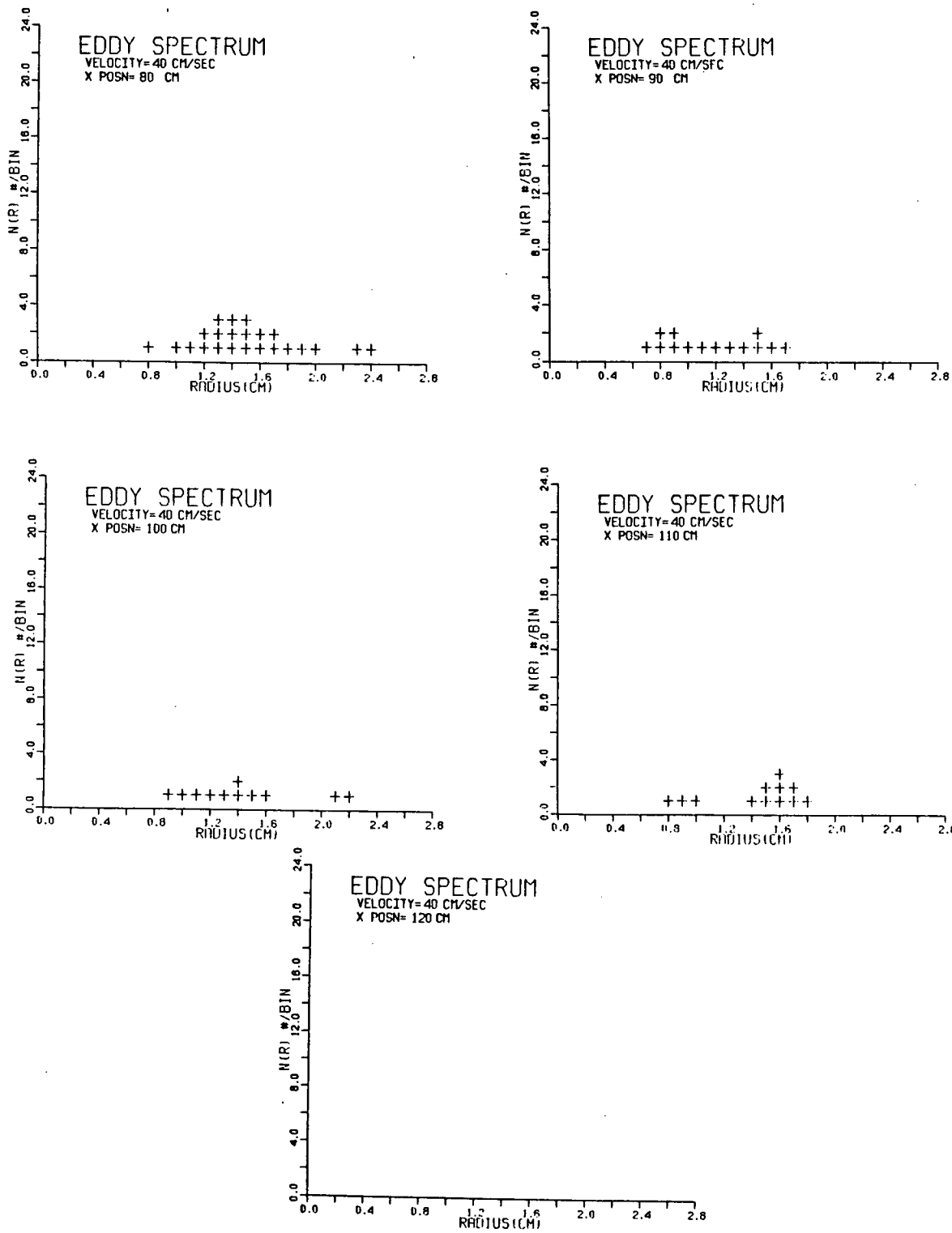

Figure 22b- 40cm/sec Eddy-Size Spectra

4.3 Generation Of E (w) From N(R)

The eddy-size distribution was used by a computer program to generate the power spectral density curves E (w). Figure 23 is a flow chart of the program and details of the Fortran IV computer code TURB.FTN are given in Appendix C. The fluctuating velocity that would be measured by a probe moving with constant velocity through the eddies was modeled and then fast fourier transform (FFT) analyzed to produce the power spectrum. Assuming an eddy rotates without internal stresses the streamwise component of the rotational velocity is simply,

$$u=U\ b/Rm \qquad (4-1)$$

where b is the impact parameter at which the probe meets the eddy, U is the peripheral velocity, and Rm is the eddy radius, see Appendix B. The eddies of figure 19 were observed in the lab reference frame. The convection velocity, Uc, used in the computer model is thus taken to be the cart speed, Ug, as the probe was mounted to the cart. From observations of the 40 cm/sec flow photographs one sees that the eddy speed measured in the lab frame is negligible compared with the cart speed. Thus, using this constant convection velocity, Uc=Ug, should not distort the model's predictions. Complications such as different eddy orientations and lengths or non-cylindrical coherent structures were ignored. The photos did not show any indication of significant vertical velocities. This was surprising because we expected the flow to quickly become

three dimensional. If the eddies were actually twisted the fluctuation statistics should not be significantly affected.

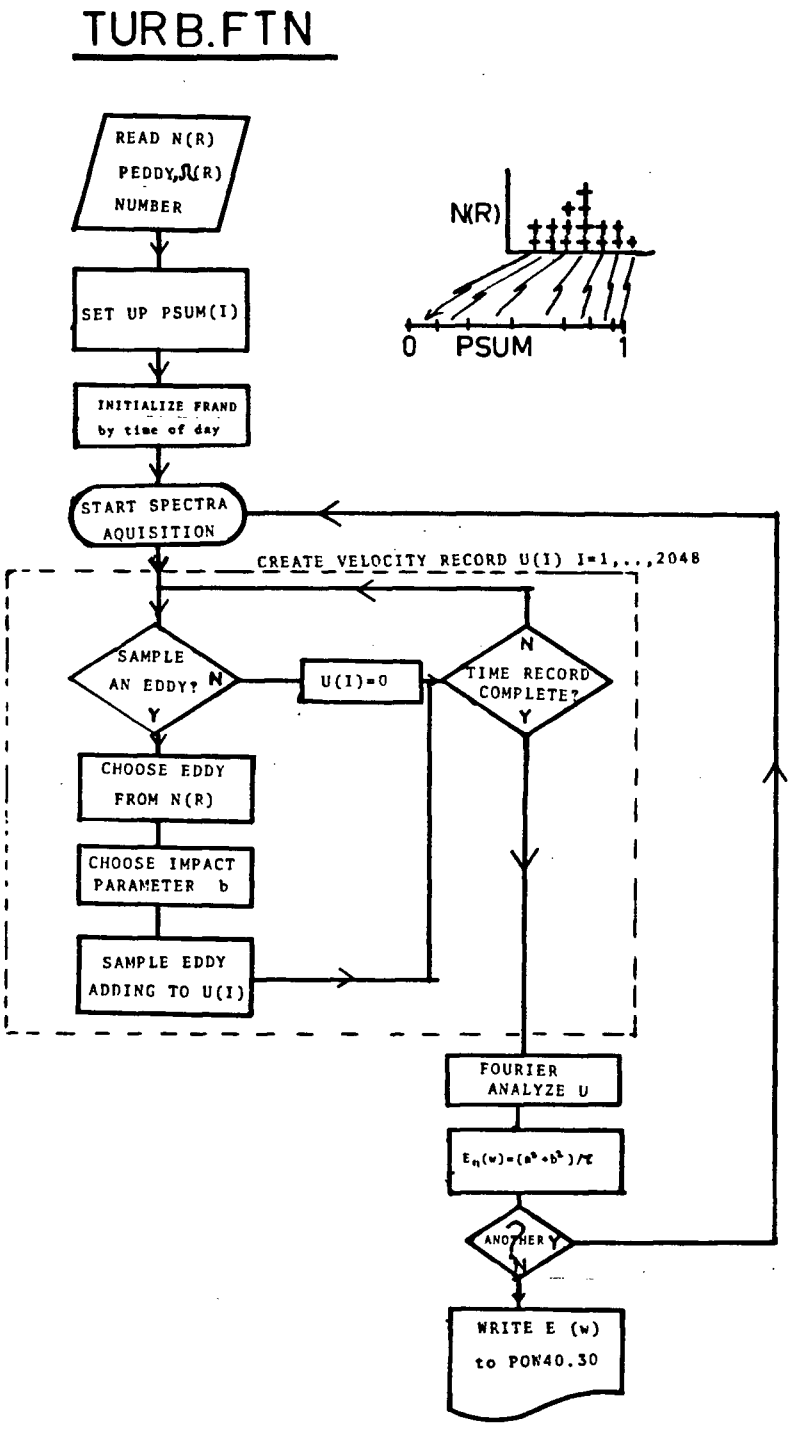

Figure 23 - N(R) to E (w) Computation

The computer code gives equal weighting to all possible eddy impact parameters b as the flow was assumed to be homogenous within a sample bin. The eddies are chosen randomly with the random number generator initialized to the time of day. Thus inter-eddy correlations were ignored.

As the eddies only take up some fraction of the sample space a 0.0cm/sec fluctuating flow velocity was randomly selected along with the probability of choosing an eddy. The probability of sampling a zero velocity rather than an eddy was chosen so that the fraction of samples with non-zero velocity would equal the observed fraction of the total bin area counted as eddies. Determining this probability requires knowledge of the average eddy length, convection velocity, sampling rate and fraction of non-zero samples required, see Appendix D.

The above assumptions of 1) eddies being randomly incident on a velocity probe which 2) measures the longitudinal component of the fluctuating velocity and 3) convecting past it at constant speed were used in the computer model to generate a fluctuating velocity time record. A typical computer generated time record is graphed in figure 24. This time record can be compared with the oscillograms of figure 15. The time interval between samples was chosen to result in a non-aliased spectrum of 0 to 100Hz frequency span. This time record was then Fourier analyzed using a UBC Computing Center library routine called DFOUR2. The Fourier coefficients were then used to

calculate the $E_{11}(w)$ according to eqn.(2-32).

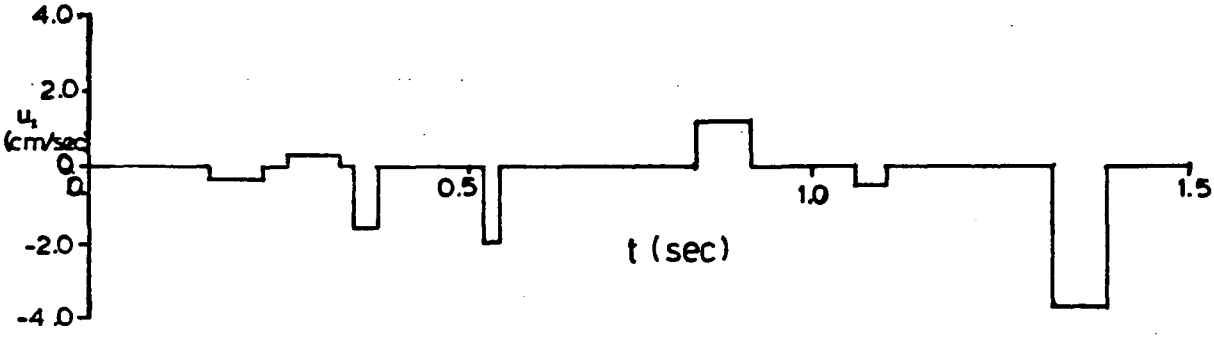

Figure 24 - $u_1(t)$ Generated from the Eddy Distribution

Having obtained an $E_{11}(w)$ spectrum a new time record is generated and analyzed. The new $E_{11}(w)$ is then averaged with the previous value. This process continues until the requested number of averages has been made. For the eddy spectra analyzed it was found that 200 averages were sufficient to define a meaningful power spectrum. Appendix C describes this entire process in detail.

The power spectral density curve was then plotted. A typical eddy power spectrum is shown in figure 25b. The eddy spectrum from which it was generated is shown in figure 25a. Figure 25c is a rescaled plot of the power spectrum 25b. The rescaling is discussed later. Figure 26 shows the 40cm/sec eddy generated power spectra as a function of distance. As eddy angular velocity measurements were only obtained for the 40cm/sec photographs, eddy power spectra could only be generated for that speed. These data are

discussed in the last section of this chapter.

4.4 Power Spectrum Obtained From U(t)

In the previous sections we have described how a power spectrum can be extracted from the eddy size distribution. These results are to be compared with power spectra obtained using the hot-film CTA, (constant temperature anemometer) and spectrum analyzer. The CTA produces a DC filtered voltage signal proportional to the streamwise velocity component. This signal is Fourier analyzed by the spectrum analyzer to produce the RMS power spectra of these voltage fluctuations. The power spectral density curve is obtained from this by multiplying by the anemometer calibration constant, squaring the result and then dividing by the analyzer's band-width.

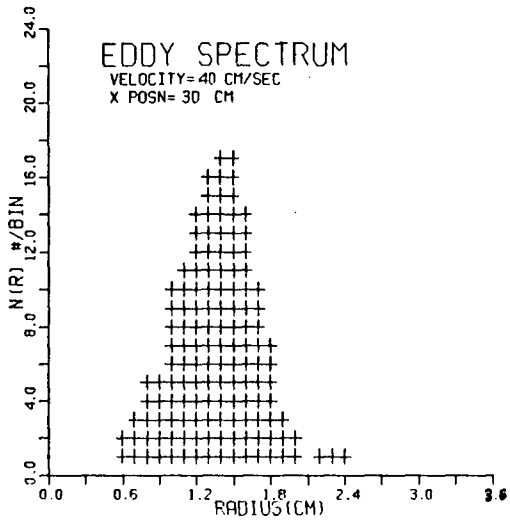

a)

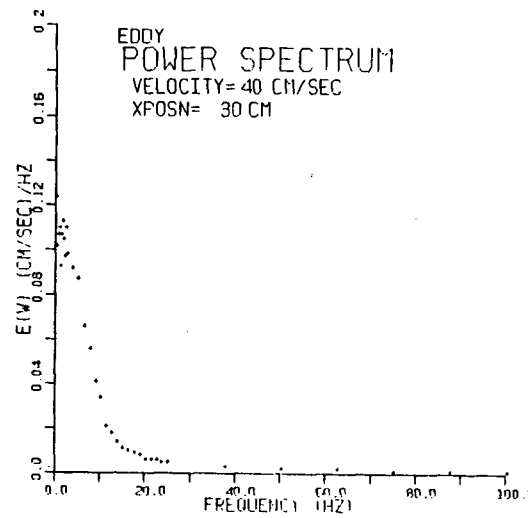

b)

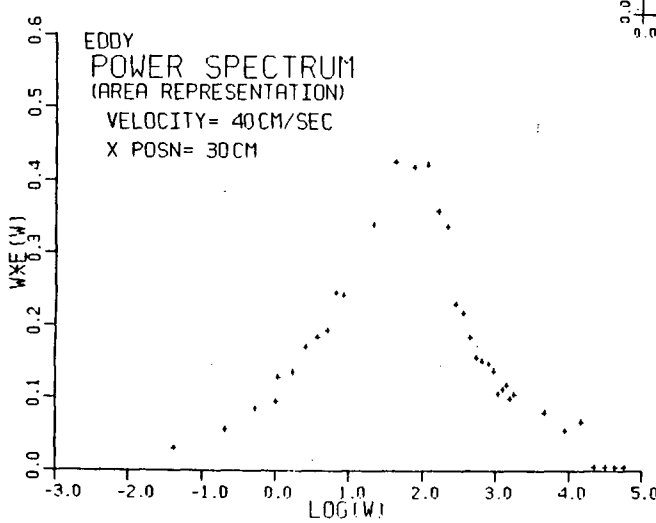

c)

Figure 25 - Eddy Power Spectra

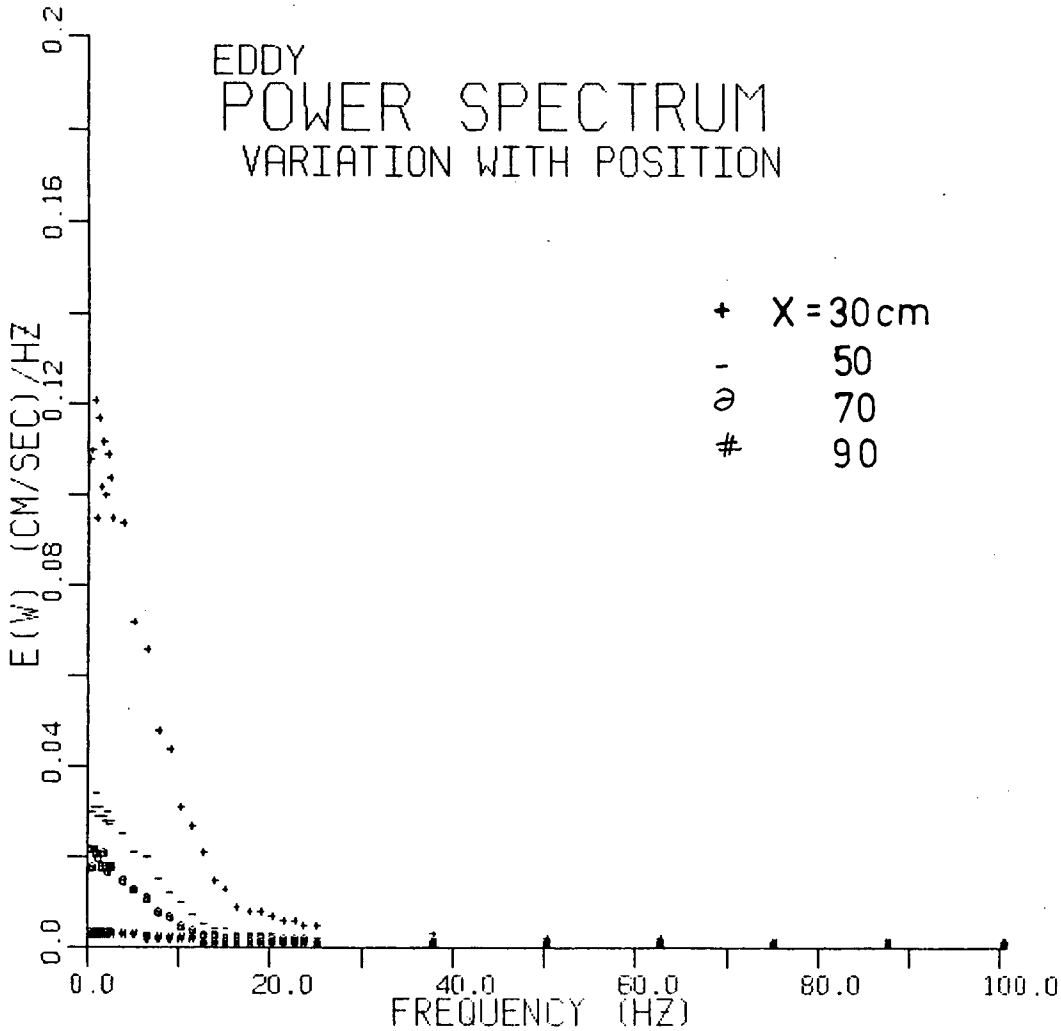

Figure 26 - Eddy Power Spectra: Variation with Distance

Figure 27 is a flow chart of how E (w) is obtained from u(t) by the spectrum analyzer. The mean voltage has been subtracted from the anemometer signal. The fluctuating voltage signal is then digitized at a rate, Fs, four times that of the maximum frequency of interest. For a 0 to 100Hz span the sampling frequency Fs is 400Hz. If u(t) contains fluctuations with frequencies greater than Fs these would be aliased to lower frequencies. However sampling at this four times higher frequency allows the potentially aliased amplitudes to be eliminated. The digitized velocity fluctuation signal is u_j $j=1,2,..,N-1$ where $N=T/Fs$ with T being the total sampling time. In practice N is predetermined due to limited available memory space and the binary operations in the FFT process. The discrete Fourier transform (DFT) of the u_j is defined as

$$A(k)=\sum_{j=0}^{N-1} u_j \exp[(2\pi i/N)(-jk)] \qquad (4\text{-}2)$$

The A(k) are the, in general, complex Fourier amplitudes for the sinusoidal basis functions with frequencies $0,1/(N\Delta t),\ldots(N-1)/(N\Delta t)$ where Δt $(=1/Fs)$ is the time interval between successive samples. In practice only the first 1/4 of these amplitudes are used as mentioned above. The absolute value of the first N/4 A(k) complex values are then squared as in eqn.(2-32) and RMS averaged to the previous spectra.

$$E_{11}(w_K)=A(k)A^*(k)/\Delta f \qquad (4\text{-}3)$$

Enough such determinations of $E_{\parallel}(w_k)$ k=0,..(N-1)/4 are made and averaged so that averaging in a new $E_{\parallel}(w)$ does not significantly change the spectrum.

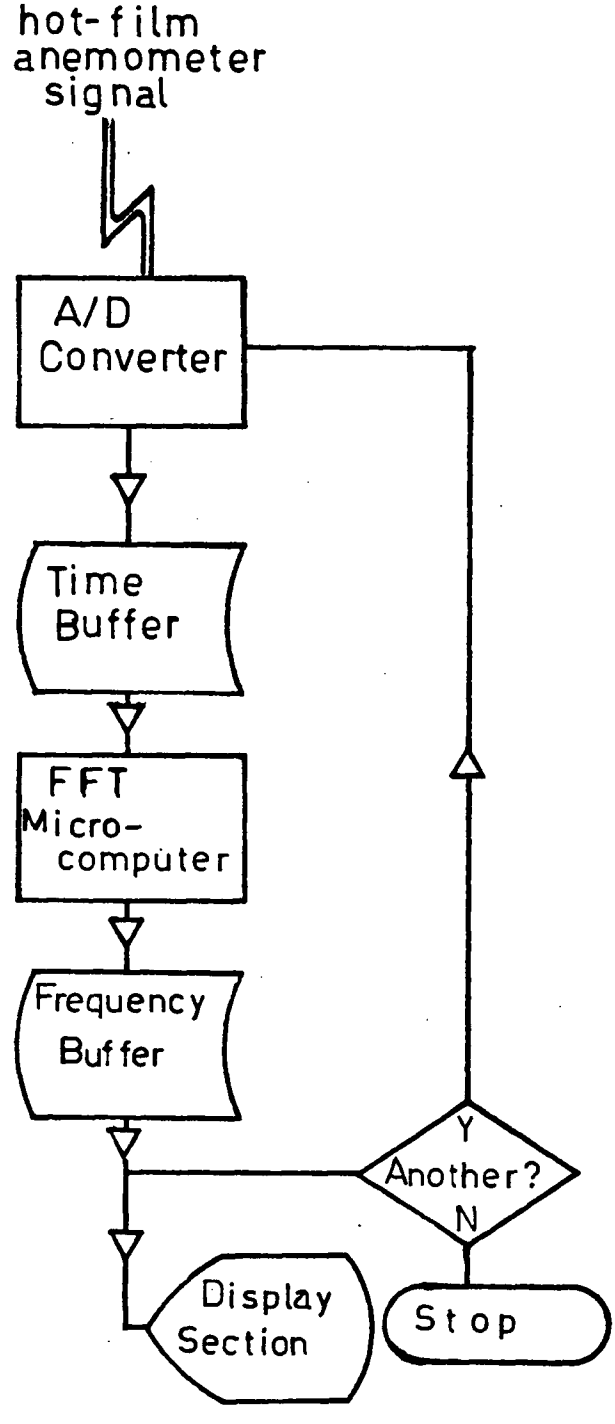

Figure 27 - Spectrum Analyzer Operation

An HP X-Y plotter was used to obtain a copy of the RMS power spectra. This plot was then digitized at the UBC Computing Center. In the digitizing process the curves were smoothed and the probe support resonance was eliminated. The RMS values were also multiplied by the calibration constant and divided by the band pass width in the digitization process. The square root of the power spectral density was thus written into a computer file. These values were then squared to obtain the hot-film measured power spectral density curve. A typical curve appears in figure 28b. The analyzer output from which it was calculated is shown in figure 28a.

Properties of the decay of turbulent fluctuations can be studied by examining the change in the power spectra with distance. Figure 29 shows the $E_{11}(w)$ spectra as a function of distance from the grid. A discussion of these spectra appears in the next section.

When comparing the power spectra obtained from the eddy-size distribution with that obtained using the hot-film anemometer one should remember that the analysis of the fluctuating signal was operationally equivalent. Indeed the computer model's method of computing and averaging succesive spectra was designed after the spectrum analyser's. For the hot-film analysis an HP 3582A spectrum analyzer was used to generate $E_{11}(w)$ from the voltage fluctuations while the

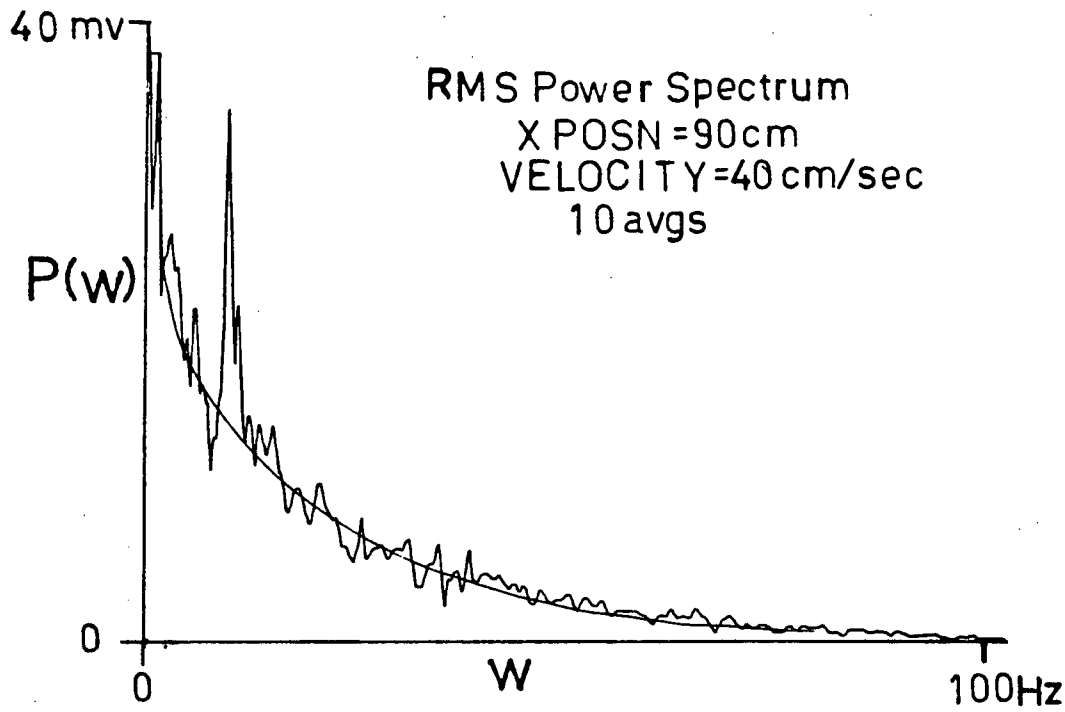

typical xy plot

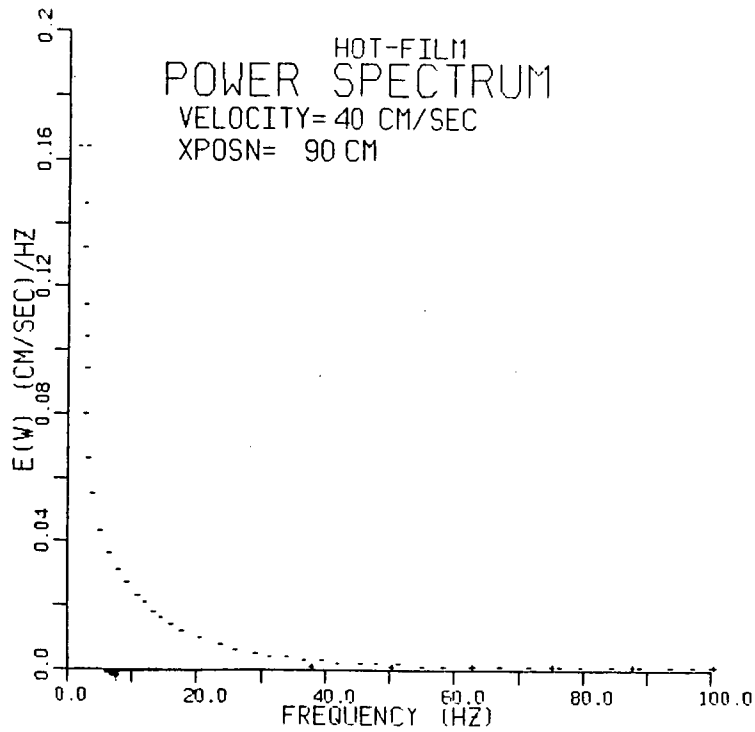

Figure 28 - Analyzer X-Y Plot

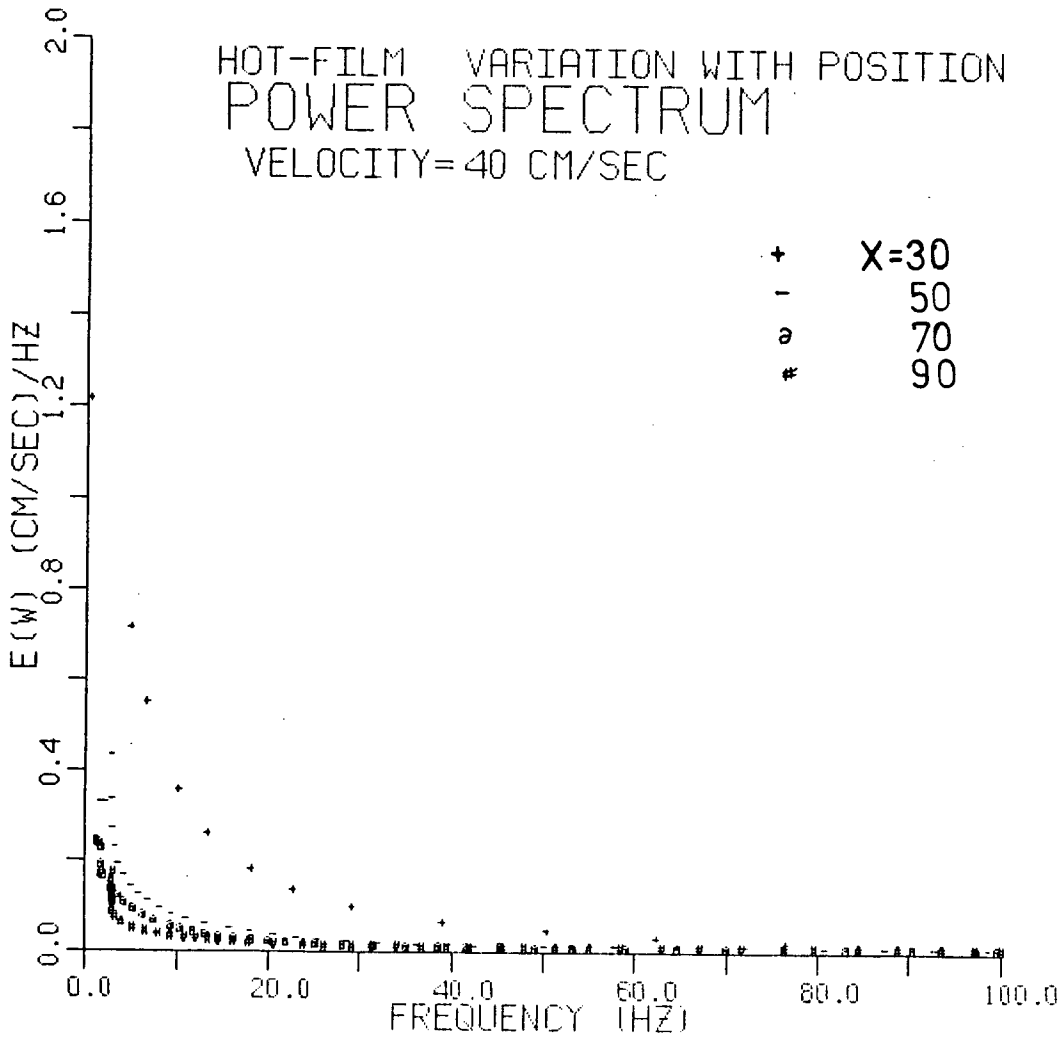

Figure 29 - Hot-Film Power Spectra: Variation with Distance

computer model used UBC Fast Fourier Transform software to achieve the same end starting with u(t) generated from the eddy-size spectrum.

4.5 Results And Discussion

The 40cm/sec eddy-size spectra were shown in figure 22. Several observations can be made from these. At a distance of 20cm behind the grid the distribution is both lower and not as peaked as at 30cm. The stress energy has not completely been converted to rotational kinetic energy of the coherent structures. 30cm from the grid the distribution is quite sharply peaked about the 1.4cm radius. The bar size and separation determine this size. As the flow evolves we see that the distribution of eddy sizes broadens and the total number of eddies decreases. Both larger and smaller size structures have evolved from the grid geometery dominated distribution. The increase in total number of eddies at the 60cm position is likely due to the small statistical sample used.

A prominent feature of the eddy-size spectra is the appearance of a second hump at a larger size radius than the initial peak. See figure 22 for X POSN=100 and 110 cm and figure 23 for X POSN=130 through to 190cm. This discontinuous increase in size is convincingly explained in terms of eddy pairing. Looking back to the flow patterns it was seen that adjacent co-rotating eddies would often appear in different stages of an evolution to a single eddy as depicted in figure 30.

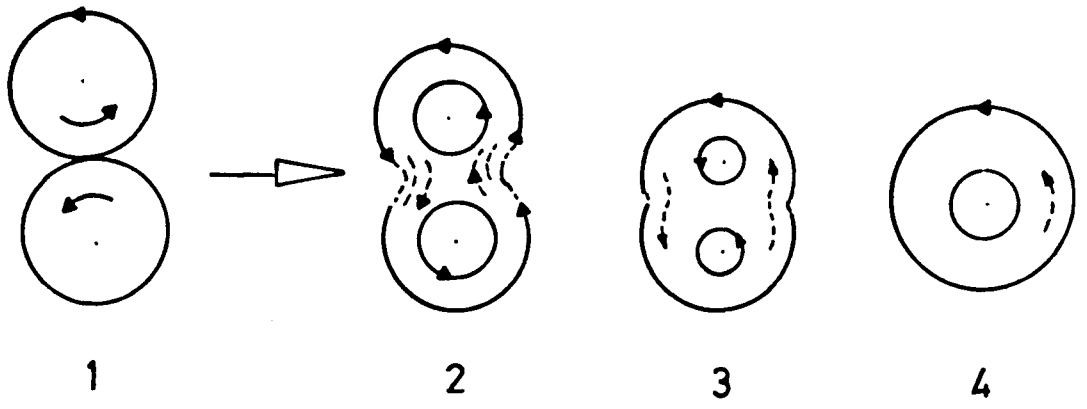

Figure 30 - Eddy Pairing

This can be understood by considering the higher pressure present in the viscously interacting boundary between the two eddies. The flow would be redirected around the interaction region to become part of the composite structure. The jump in eddy size is thus observed.

It is well worth gazing at the flow patterns of figures 9 through 12. One soon realizes that many coherent structures persist in successive photographs. This further supports our use of Taylor's hypothesis. Imaginative scrutiny of the succesive flow patterns show the evolution of the eddies both individually and organizationally. Our flow visualization technic is seen to be an effective tool for studying eddy dynamics.

The average chord length of an eddy can be calculated from the eddy distributions, see Appendix D. This length is compared with the integral length scale derived from both the eddy spectra and the hot-film power spectra in figure

31. A discussion of these results appears later in this section. The total number of eddies observed as a function of distance is plotted in figure 32 for the 40cm/sec data.

The eddy produced spectra appear with their corresponding hot-film measured curves in figure 35. The uncertainty in the eddy curves is largely due to the uncertainty in the angular velocity of the eddies. This is seen from figure 20 to be about 25%. The hot-film curve's uncertainty due to calibration drift and mechanical resonance is about 15%. The statistical uncertainty due to insufficient spectra averaging can be estimated by observing the effect of averaging succesive spectra during the aquisition process. An uncertainty of 10% for the 25Hz range, increasing with decreasing frequency is a reasonable estimate.

The eddy curves are seen to be consistently lower than the corresponding hot-film spectra. The frequencies containing appreciable energy are also consistently lower for the eddy generated spectra. Possible reasons for this are several. Inspection of figure 19a shows that only about 1/5 of the total area of the flow has been characterized as eddies while almost all of the flow seems to be agitated. The local flow velocity in the regions between the eddies is about as large as the rotational velocity at the edqe of the eddies, hence the inter-eddy fluid contains about as much kinetic energy per unit mass as the eddies. The ratio of the total eddy area to the bin area, figure 33, is therfore

a good measure for the fraction of the total kinetic energy of the flow stored in the eddies.

The flow between the eddies was contains substantial velocity changes. This is seen in the oscillograms of figure 15 as well. These fluctuations have not been accounted for in our simple analysis. The velocity changes in the eddy interaction regions occur over distances often substantially shorter than the typical eddy size. A Fourier decomposition of the flow field taking these regions into account would show more energy in higher frequencies than our analysis. Another explanation of the lack of energy in the higher frequencies is the size scale resolution limit of both the visualization and analysis methods used. A large photographic print of the flow showed some smaller scale coherent structures which were not counted when the projection system was used. The low tracer density could also cause us to miss the smaller scale eddies however from observation of the flow photographs it was concluded that for all but the 50cm/sec cart speed the spatial resolution was adequate.

In generating the eddy power spectra any explicit inter-eddy correlations were ignored. Observation of the flow patterns showed the presence of clumps of eddies separated by "rivers" of relaminarized flow. Adjacent co-rotating eddies would contribute to the low frequencies of the Fourier analysis. Electrical noise in the hot-film diagnostic system as well as unaccounted for mechanical

vibrations would contribute to the hot-film spectrum. A constant low frequency non-turbulent noise in the anemometer signal would also explain the increasing discrepancy with distance in the low frequency regime. Increasing intereddy correlations or counting the circular core of a large non-circular structure could also explain this. There is not enough information to decide what to attribute the discrepancy in the spectra to although more than enough to speculate. Suffice to say that a significant fraction of the fluctuating kinetic energy in the proper frequency regime is predicted from our simple eddy description of the fluctuations. It would be useful to analyze the flow photos again and treat lumps of fluid with a common rotation axis as incomplete eddies. This would account for all the flow field in a straightforward manner.

The total mean square of the longitudinal velocity fluctuations is found by integrating E (w), as shown in eqn.(2-23).

$$\overline{u^2} = \int_0^\infty E_u(w)\,dw$$

Figure 34 shows the decay of $\overline{u_1^2}$ with distance X for both the fluctuations generated by the eddy spectrum and the fluctuations measured from the hot-film anemometer. The "eddy" u values have been multiplied by a factor of 10.0 to facilitate a comparison in the energy decay trend. The remarkable similarity in the decay trends indicates that our eddy spectrum description is intimately linked with the fluctuation dynamics.

The integral length scale can be obtained from the power spectra using eqn (2-26).

$$Le=UcE_{u}(0)/(4\overline{u_1^2})$$

This length scale should be related to the size of the eddies. Figure 31 shows the average eddy chord plotted against distance X together with twice the integral length scales obtained from the eddy produced and hot-film measured power spectral density curves. The similarity between the average eddy chord and the eddy produced spectrum's integral length scale is not remarkable except that it tells us that twice the integral length scale should be associated with the average eddy size. The similarity between the hot-film measured and eddy spectrum produced integral length scales is quite good for the first three distances. This tells us that the eddy spectrum description has characterized the size scale of the energy containing fluctuations quite well in spite of our crude analysis. The divergence of the hot-film integral length scale at the 90cm distance is related to the anomalously high energy content in the low frequency end of the 90cm curve of figure 35. Speculations of constant background noise or influence of inter-eddy correlations have been mentioned. Although it is also quite likeky that this anomoly is due to erroneous digitizing.

To study contributions to the fluctuating kinetic energy in different frequency regimes the power spectra were rescaled to expand the frequency axis. This was done by plotting $wE_{uu}(w)$ against log(w). The new curve has equal

areas representing equal contributions to the total turbulent kinetic energy. This can be seen by observing that the integral representing the area under $wE_{11}(w)$ between two logged frequency axis points $\log(w_1)$ and $\log(w_2)$ simplifies to the integral of $E_{11}(w)$ between the corresponding frequencies,

$$\int_{\log(\omega_1)}^{\log(\omega_2)} wE_{11}(w)\, d\{\log(w)\} = \int_{\omega_1}^{\omega_2} E_{11}(w)dw \quad \text{as} \quad wd\{\log(w)\} = w/wdw = dw \qquad (4\text{-}4)$$

The expansion of the frequency scale facilitates the study of trends in different frequency regimes. Figure 36 compares the same spectra now plotted in the new format. The frequency axis point corresponding to the integeral time scale is where w=1/Te at log(Te). It has been marked on the figures and is near to where the maximum contribution to the total energy occurs. This agrees with our interpretation of Te as a measure of the time scale of the energy containing fluctuations. This area representation is best used when differences in the distribution of energy among different frequency regimes are of interest. In the new representation we can more clearly see that the eddy generated power spectral density is more sharply peaked than the hot-film curve. This is due to the highly simplified eddy analysis that was used. The intra-eddy velocity distributions were highly idealized and the angular velocity distributions were over simplified to be a constant for a given distance from the grid. Had the measured distribution in angular velocities been used instead of the average value

a broader distribution of energy about the integral length scale would be expected.

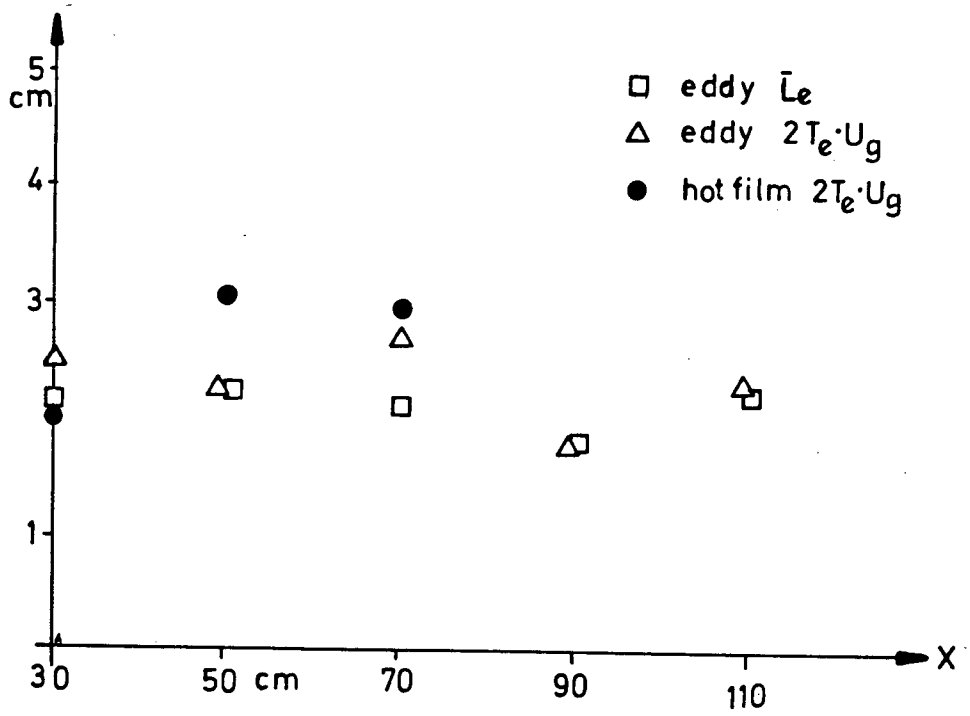

Figure 31 - Comparison of Length Scales

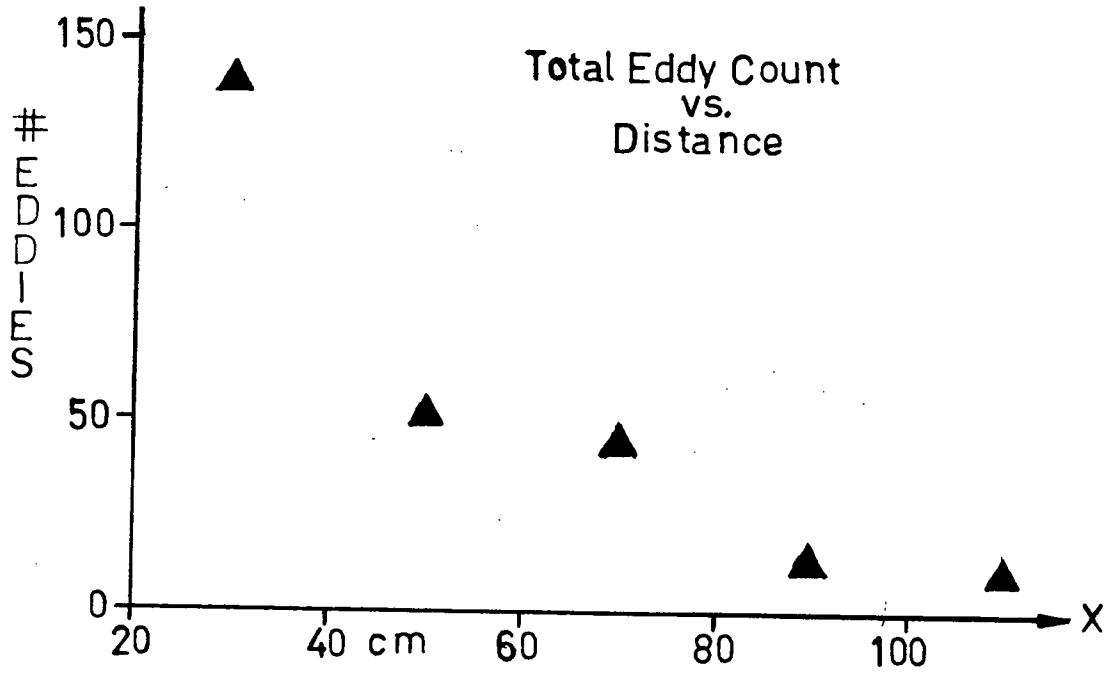

Figure 32 - Eddy Count with Distance

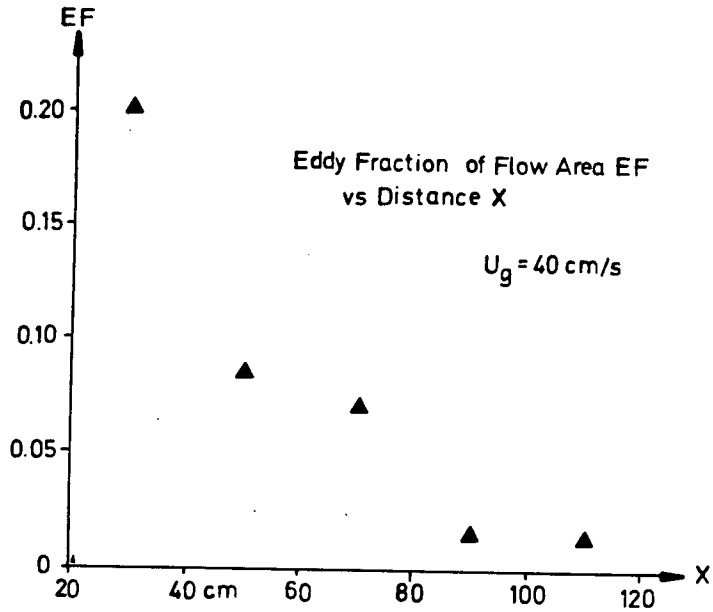

Figure 33 - Variation in Occupied Area

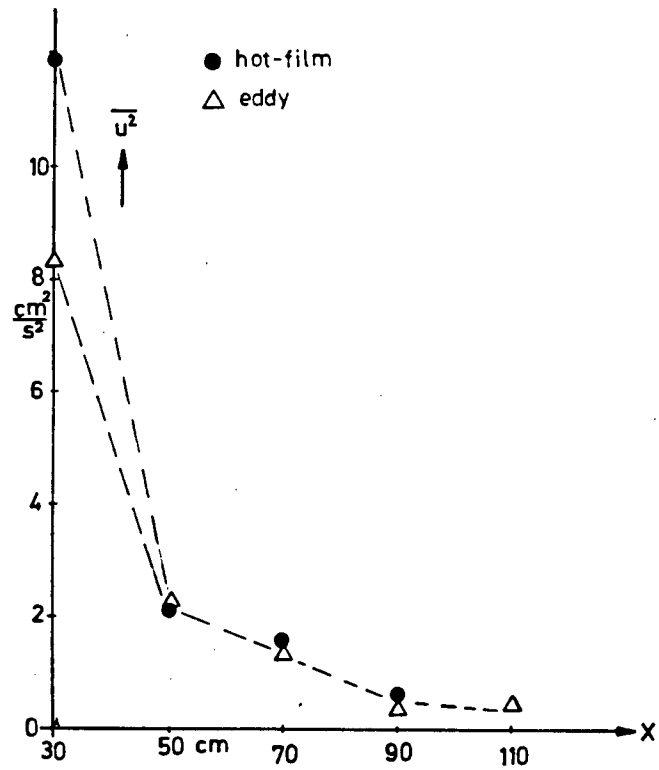

Figure-34 Decay of $\overline{u^2}$

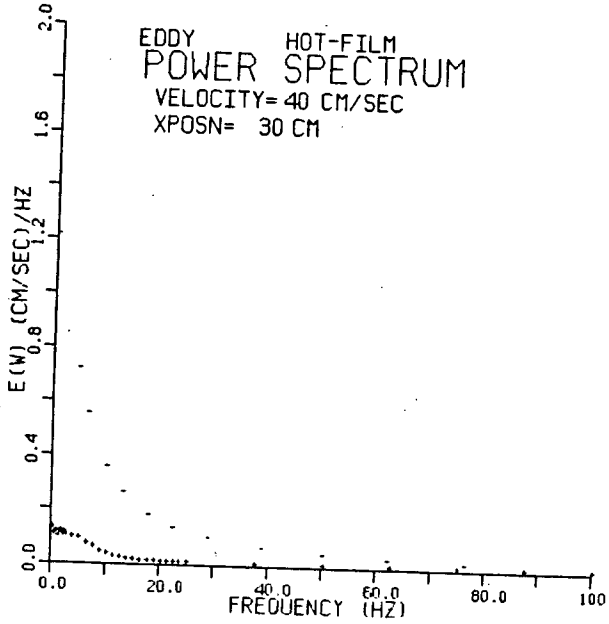

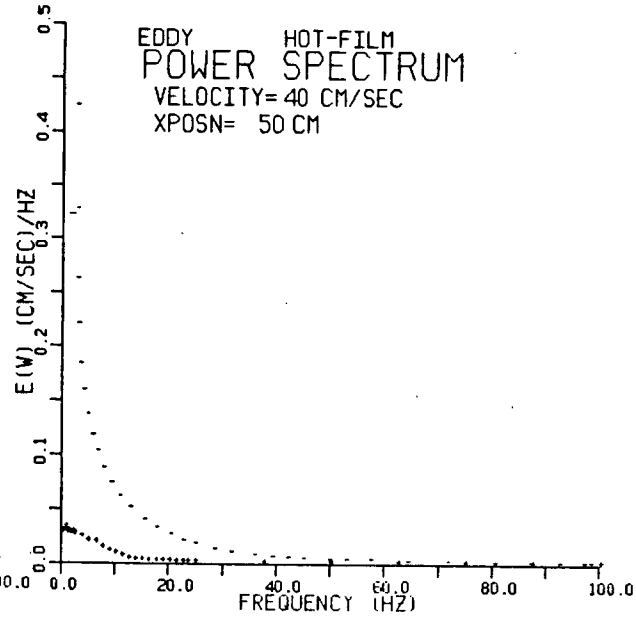

+ eddy
- hot-film

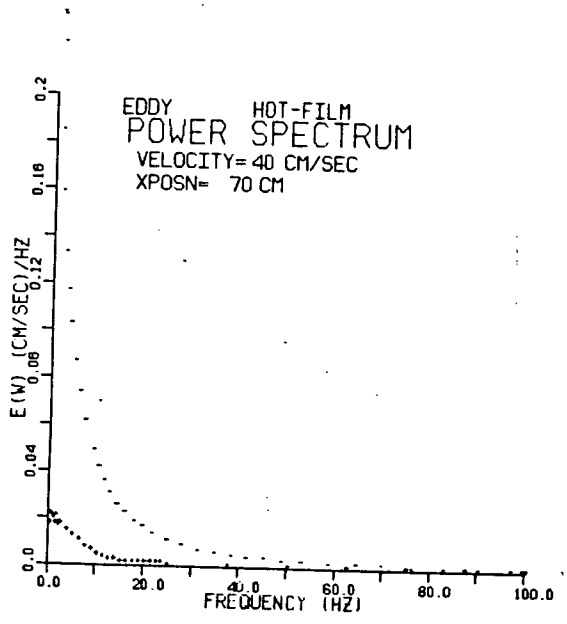

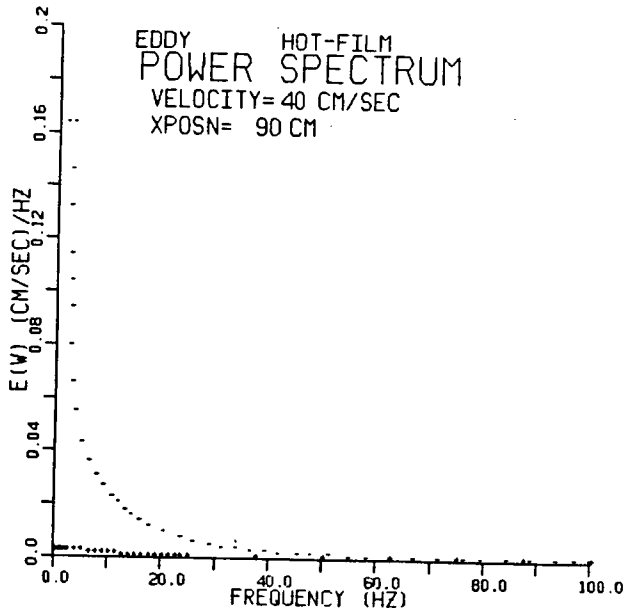

Figure 35 - Comparison of Power Spectra

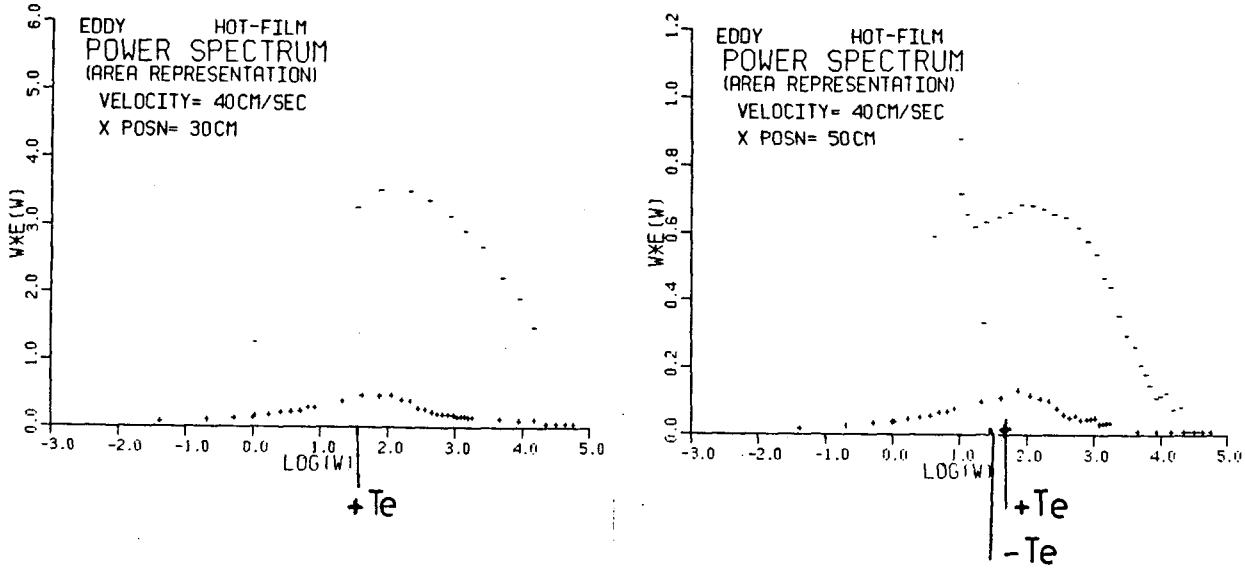

+ eddy
- hot-film

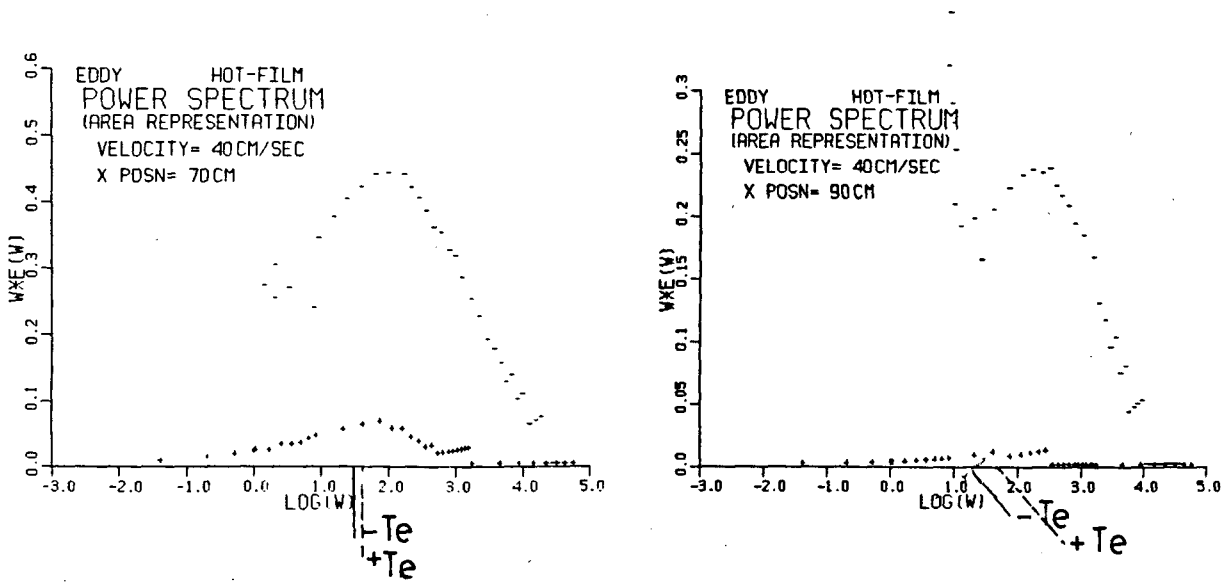

Figure 36 - Equivalent Area Representation

V. CONCLUSIONS

A model which treats a turbulent flow as being composed of coherent rotations plus laminar flow has been presented. Experiments were performed to study how well this model describes the velocity fluctuations in a grid generated turbulent flow. We searched for and found coherent structures by photographing the motions of aluminum tracers. The towing tank constructed for these experiments allowed for easy access to either the fluid or object reference frame. Although the fluid velocity information is available from both frames it was found that the visualization technique was only useful with the camera in the fluid reference frame.

The distribution of sizes and angular velocities of the eddies were measured from these photographs. This eddy-size spectrum was used to generate the power spectral density of the longitudinal velocity fluctuations.

A hot-film anemometer was used to measure the longitudinal velocity fluctuations generated by the grid. A spectrum analyzer produced the power spectral density from these fluctuations. By comparing the hot-film measured and eddy spectrum generated power spectral densities we have drawn the following conclusions:

The eddy-spectrum description predicts the size scales of the turbulent fluctuations. It also predicted a constant 10% of the total kinetic energy of velocity fluctuations measured by the hot-film probe. The eddy model was least

successful at describing the kinetic energy in the high and low frequency regimes. We believe this discrepancy is partly due to the fact that inter-eddy correlations and coherent fluctuations in the space between the eddies were not accounted for in our analysis. Our simple treatment of the velocity profile within an eddy may have contributed as well.

The eddy-size spectrum proved useful for understanding the dynamics of the evolution of turbulent length scales. The evolution of the structures could be seen in successive flow photographs. Evidence of eddy-pairing was observed for co-rotating structures both in the eddy-size spectrum's evolution and in the flow photographs. We look forward to learning more about eddy interactions by studying sequential photographs of fluid flow patterns.

Our model has many advantages over the usual statistical description of turbulence. As this thesis has shown coherent structures can be observed in and are important to the dynamics of turbulent fluid flow. A description of turbulence in terms of eddy spectra is simpler to understand and more physically motivated than studying "statistical fluctuations". This description naturally takes into account the mechanics of coherent structures. Also, the eddy-dynamics could be useful for predicting properties of turbulent flows such as the influence of turbulence on mean velocity profiles, on the

drag of a body, and on mixing processes.[1] And, of course, knowledge of the eddy dynamics can be used to predict the eddy statistics which in turn can be used to predict velocity fluctuations in a turbulent flow.

Perhaps the greatest advantage of studying turbulence from a coherent structures viewpoint is in the new understanding of the mechanics of turbulent flows that may arise. Aside from its aesthetic value understanding the mechanics of eddy production could lead to more efficient fluid machinery by influencing the production and decay of coherent structures. More efficient canoes and sailboats not to mention freighters and aircraft could be possible.

The results of this thesis indicate that developing better criteria for analyzing structures in the flow would be worthwhile. This could be done by analyzing an entire three dimensional flow field concentrating on the local curvature and angular velocity. This analysis would address the observed phenomenon of partly formed, or fractional, eddis. An automated analysis using a digitized video signal would be quite straightforward to implement using this definition. Many flows could then be analyzed in a rigorous fashion.

---

[1] UBC PLASMA PHYSICS lab report #89

BIBLIOGRAPHY

B.Ahlborn, F.Ahlborn and S.Loewen: UBC PLASMA PHYSICS lab report #89, (1983)

F.Ahlborn: Zeitschrift fur Technische Physik 12 , 482-491 (1931)

J.O.HINZE: TURBULENCE, McGRAW-HILL, (1959)

J.L.LUMELY: Stochastic Tools in Turbulence, Academic Press, (1970)

Roberson and Crowe: Engineering Fluid Mechanics, Houghton Mifflin Co., (1975)

H.Tennekes and J.L.Lumley: A First Course in Turbulence, MIT Press,(1972)

APPENDIX A - HOT-FILM PROBE SENSITIVITY TO VELOCITY FLUCTUATIONS

Ignoring this influence the probe will respond to the speed of flow past the sensor. For a linearized probe the flow speed S is related to the linearized anemometer voltage signal, E , by the relation

$$S=KE \qquad (A-1)$$

where K is the calibration constant. The flow speed S is related to the flow velocity components by the relation

$$S^2=(U+u)^2+v^2+w^2 \quad V=W=0 \qquad (A-2)$$

where u,v,w are the longitudinal and two lateral fluctuating velocity components and U is the longitudinal mean velocity component. Writing out the (U+u) term we have

$$S^2=U^2+2Uu+u^2+v^2+w^2 \qquad (A-3)$$

If the turbulence intensity is sufficiently low so that $u,v,w \ll U$ the squared terms in eqn.(3-3) may be neglected. After dividing both sides by U and taking their square root we have

$$S/U=/1+2u/U \qquad (A-4)$$

Now using a Maclaurin series expansion for the square root with $u \ll U$ and multiplying by U we have

$$S=U+u \qquad (A-5)$$

Treating the linearized voltage E as the sum of a steady, E , plus a fluctuating component, e, and substituting eqn.(A-5) into eqn.(A-1) we see that

$$U+u=KE+Ke \qquad (A-6)$$

The fluctuating part of the anemometer signal is proportional to the fluctuating part of longitudinal velocity. The constant of proportionality being the same as the calibration constant for the mean component. The wedge shape of the probe tends to suppress the v and w velocity component contributions to the cooling thus further reinforcing equation (A-6).

APPENDIX B - RIGID BODY EDDY VELOCITY PROFILE

A rigid body circularly cylindrical eddy of radius Rm rotating about its axis of symmetry has a velocity profile given by

$$u_\theta(r)=Um(r/Rm) \quad 0<r<Rm \tag{B-1}$$

where Um is the tangential velocity at the periphery of the eddy and r is the radius, see figure below. The u_1 component of the velocity is given by,

$$u_1=u_\theta \, r\sin\theta \tag{B-2}$$

and using equation B-1 becomes

$$u_1=(Um/Rm)r\sin\theta \tag{B-3}$$

If a u component velocity probe moves through the eddy at constant speed in the x direction, as shown, with impact parameter b we have

$$r\sin\theta=b \tag{B-4}$$

so that equation B-3 becomes

$$u_1=(Umb/Rm) \tag{B-5}$$

showing that the fluctuating component of the velocity for a rigid body eddies is a constant. A little study of the figure below shows that the sampling time through the eddy would be given by

$$t=(2/Uc)\{Rm^2-b^2\} \tag{B-6}$$

with Uc being the probe speed relative to the eddy.

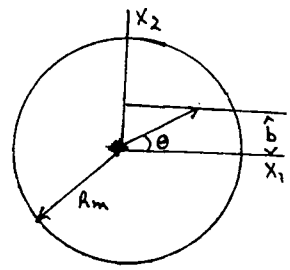

APPENDIX C - TURB.FTN FORTRAN CODE

```
      C  TURB.FTN
      C  INPUT DATA ON UNIT 11
      C  OUTPUT DATA ON UNIT 6
      C
      C  PROGRAM CHANGES EDDY SPECTRUM TO POWER SPECTRUM
      C
      C  EDDY CHARACTERIZING DISTRIBUTIONS ARE READ IN
      C
      C
            INTEGER  NLNGTH, NVEL, NCONV, NPTS, N1PTS, MPTS, NRMAX, NRNOT
            INTEGER J, I, CHOOSE, M, NUMBER, NDATA, NUX, SUMNUX
            INTEGER LOGSPC(37) /1, 2, 3, 4, 5, 6, 7, 8, 9, 10, 11,16, 21,
           1        27,32,37,42,47,52,57,62,67,73,78,83,88,93,97,103,155,206,
           2        257,308,359,411,462,513/
            REAL NR(500), RNOT(500), RMAX(500), VEL(500), RAD(500)
            REAL CONVEL(500),PSUM(500) ,ENERGY/0./,AREA/0./,TE/0./
            REAL LEBAR, RCHOSE, RMAXO, RNOTO, B, CONVEC, TSTEP, TRATE
            REAL NL(500), L(500), UX(6000), UMAX(500), RATIO, TEMP
            REAL POWER(1025) /1025*0./, FREQ(1025), REALI
            REAL*8 DATA(2048)
            COMPLEX*16 TRAN(1025)
            EQUIVALENCE (DATA(1),TRAN(1))
      C  READ FILE NUMBER
            READ (11,230) SPECN
      C  READ SAMPLING FREQUENCY
            READ (11,260) TRATE
      C  TRATE=FREQUENCY RESOLUTION/NYQUIST CRITERIA
      C
      C  NUMBER IS NUMBER OF RMS AVERAGES TO BE MADE
            READ (11,210) NUMBER
      C  READ PEDDY ET AL
            READ(11,320)PEDDY,AREA,LEBAR,NUMED
      C  READ IN EDDY SIZE SPECTRUM
            READ (11,210) NRMAX
            DO 10 J = 1, NRMAX
              READ (11,270) NR(J), RMAX(J), RNOT(J), UMAX(J)
         10 CONTINUE
      C  READ IN CONVECTION VELOCITIES
      C
         60 READ (11,210) NCONV
            IF (NCONV .EQ. 1) GO TO 80
            DO 70 J = 1, NCONV
              READ (11,230) CONVEL(J)
         70 CONTINUE
         80 READ (11,230) CONVEC
      C
      C  PREPARE SIZE DISTRIBUTION FOR RANDOM SAMPLING
      C
      C  INITIALIZE FRAND BY TIME-OF-DAY
            B = RAND(SCLOCK(0.))
            PSUM(1) = 0.
            MPTS = NRMAX - 1
            DO 90 I = 1, MPTS
              PSUM(I + 1) = PSUM(I) + NR(I)*2*RMAX(I)
         90 CONTINUE
            DO 100 I = 1, NRMAX
              PSUM(I) = PSUM(I) / PSUM(NRMAX)
        100 CONTINUE
      C
      C  SAMPLING LOOP STARTS
```

```
      C
            PBLANK=1.-PEDDY
            DO 190 K = 1, NUMBER
              USQBAR=0.
              SUMNUX = 0.
      C  NDATA IS NUMBER OF VELOCITY SAMPLES TAKEN
      C  PER FOURIER ANALYZED RECORD
              NDATA = 2048
      C     TIME RECORD BEING MADE
      C   CHOOSE UX=0. OR SAMPLE AN EDDY
        105   X=FRAND(0.)
              IF (X.GT.PBLANK) GOTO 110
              SUMNUX=SUMNUX+1
              DATA(SUMNUX)=0.
              IF (SUMNUX.GT.NDATA)GOTO 170
              GOTO 105
      C     CHOOSE EDDY RADIUS
        110   IRAD = CHOOSE(M,PSUM,NRMAX,RCHOSE)
              RMAXO = RMAX(IRAD)
              RNOTO = RNOT(IRAD)
      C     CHOOSE IMPACT PARAMETER
        130   B = 2. * (FRAND(0.) - .5) * RMAXO
      C     FIND CONVECTION VELOCITY
              IF (NCONV .GT. 1) CONVEC = CONVEL(IRAD)
        140   CALL SAMPLE(TRATE, RNOTO, RMAXO, UMAX(IRAD), B, CONVEC, NUX,UX)
              DO 150 I = 1, NUX
                IF (I + SUMNUX .GT. NDATA) GO TO 170
                DATA(I + SUMNUX) = UX(I)
                USQBAR=USQBAR+UX(I)*UX(I)
        150   CONTINUE
        160   SUMNUX = SUMNUX + NUX
              GO TO 105
      C  WRITE OUT TIME RECORD IF WANTED
      C 170   WRITE(9,370)(DATA(II),II=1,2000)
        170   ENERGY=ENERGY+USQBAR/NDATA/NUMBER
      C  DFOUR2 FOURIER ANALYZES THE TIME RECORD
              NDIM = NDATA
      C  NODIM=  # OF DIMENSIONS OF TIME RECORD
              NODIM = 1
      C  ISIGN=-1 FOR DFT +1 FOR IDFT
              ISIGN = -1
      C  IFORM=0 FOR REAL DATA
              IFORM = 0
              CALL DFOUR2(DATA, NDIM, NODIM, ISIGN, IFORM)
              DO 180 I = 1, 1025
              POWER(I) = POWER(I) + ((CDABS(TRAN(I))/NDATA)**2)/NUMBER
        180   CONTINUE
        190 CONTINUE
            TSTEP = 1. / TRATE
            DO 200 I = 1, 1025
              REALI = FLOAT(I)
              FREQ(I) = (REALI - 1.) / (NDATA*TSTEP)
        200 CONTINUE
            AREA=QINT4P(FREQ,POWER,513,1,513)
            TE=POWER(1)/(4.*AREA)
            DO 202 KK=1,513
            POWER(KK)=POWER(KK)*9.8696
        202 CONTINUE
            N1PTS = 35
            WRITE (6,280) SPECN, CONVEC, N1PTS, ENERGY,TE
```

```
      WRITE (6,300) (POWER(LOGSPC(I)),FREQ(LOGSPC(I)),I=1,N1PTS)
      STOP
C     FORMAT CODES
  210 FORMAT (I3)
  220 FORMAT (2I3)
  230 FORMAT (F7.3)
  240 FORMAT (2F7.3)
  250 FORMAT (3F7.3)
  260 FORMAT (F5.0)
  270 FORMAT (4F7.3)
  280 FORMAT (F7.3,F7.2, I3,F7.4,E10.3)
  290 FORMAT (3(D16.9,F5.0))
  300 FORMAT (3(F10.3, F9.3))
  310 FORMAT (3(F10.3,F9.3))
  320 FORMAT (F7.5,2F7.3,I3)
  370 FORMAT(10F9.3)
      END
      INTEGER FUNCTION CHOOSE(M,PSUM,NRMAX,RCHOSE)
C  THIS PROGRAM RANDOMLY CHOOSES AN INTERVAL FROM A
C  PREDETERMINED DISTRIBUTION
C  M IS THE INTEGER NUMBER OF THE INTERVAL CHOSEN
      REAL PSUM(500), RCHOSE
      INTEGER M, NPTS, SCOPE, MPTS
      LOGICAL GT, LT
      MPTS=NRMAX-1
      M = NRMAX / 2
      SCOPE = M + 1
      RCHOSE = FRAND(0.)
   10 GT = .FALSE.
      LT = .FALSE.
      IF (RCHOSE .GT. PSUM(M)) GT = .TRUE.
      IF (RCHOSE .LT. PSUM(M + 1)) LT = .TRUE.
      IF (LT .AND. GT) GO TO 20
      SCOPE = SCOPE / 2 + 1
      M = M + SCOPE
      IF (LT) M = M - (2*SCOPE) + 1
      IF (M.LT.1) M=1
      IF (M.GT.MPTS) M=MPTS
      GO TO 10
   20 CHOOSE = M
      RETURN
      END
      SUBROUTINE SAMPLE(TRATE, RNOTO, RMAXO, UMAX, B, CONV, NUX, UX)
C        SAMPLES UX FOR GIVEN EDDY
      INTEGER  NCORE, NUX, I
      REAL TIME, TMAX,  RMAXO, UMAX, B, CONV, UX(6000)
      REAL TRATE, TSTEP
      TSTEP = 1. / TRATE
      TMAX = SQRT(RMAXO*RMAXO - B*B) / CONV
      UCONST = UMAX * B / RMAXO
      NCORE =2*TMAX / TSTEP
 174.5
      NUX=NCORE
      DO 30 I = 1, NCORE
        UX(I) = UCONST
   30 CONTINUE
   40 RETURN
      END
End of file
```

APPENDIX D - AVERAGE EDDY CHORD AND PEDDY CALCULATION

For a circularly cylindrical eddy having a random impact parameter b with a probe the average chord, L, is the width of a rectangle with length 2Rm having an area equal to that of the eddy's circular cross section.

$$L\{2Rm\}=\pi R_m^2 \qquad (D-1)$$

so that

$$L=(\pi/2)Rm \qquad (D-2)$$

With a distribution of eddy sizes N(Rm) the average chord of all eddies randomly incident on the probe will be

$$Led=[\sum_{Rm} N(Rm)\{Rm\,\pi/2\}]/[\sum_{Rm} N(Rm)] \qquad (D-3)$$

To recreate a randomly distributed velocity record composed of zero and eddy contributions choose 0.velocity or sample an eddy velocity profile according to

Pe=probability of choosing an eddy
Po=probability of choosing a zero velocity
Ls=average number of velocity samples for the eddies
Lb=number of velocity samples when a zero is chosen (=1)
Frac=fraction of sample area taken by eddies The number of velocity samples for a length X and velocity probe speed Uc is given by (X/Uc)Fs where Fs is the sampling frequency. We first have

$$Pe+Po=1 \qquad (D-4)$$

and

$$\frac{LePe}{LePe+LoPo} = Frac \qquad (D-5)$$

so that

$$Pe=\frac{LoxFrac}{\{Le(1-Frac)+LoxFrac\}} \qquad (D-6)$$

is the probability of choosing an eddy which will randomly recreate observed eddy fraction Frac.